Carbon Nanotubes (CNTs) as Electron Emitters for Plasmas Operating in Subatmospheric pressure under DC and Pulsed Fields

by

Huirong Li

A dissertation submitted to the Graduate Faculty of
Auburn University
in partial fulfillment of the
requirements for the Degree of
Doctor of Philosophy

Auburn, Alabama
August 2, 2014

Keywords: carbon nanotubes, subatmospheric plasma,
microplasma, pseudospark switch, field emission

Approved by

Hulya Kirkici, Chair, Professor of Electrical and Computer Engineering
Michael Baginski, Associate Professor of Electrical and Computer Engineering
Thomas Baginski, Professor of Electrical and Computer Engineering
Bogdan Wilamowski, Professor of Electrical and Computer Engineering

Abstract

Subatmospheric pressure is defined as the pressure from several milliTorr to several hundred Torr. The plasmas operated in subatmospheric pressure have the advantages of easier construction and stable operation. The efficiency of the emitter electrons is critical in the performance of the plasma devices. After accelerated in the electric field between the cathode and the anode, the seed electrons play a significant role in the ionization processes. In this dissertation, two specific types of plasma devices are operated at subatmospheric pressure. The first is a in-house built microplasma device with different cathode geometry. The second is a pseudospark switch based on plasma ignition.

Microplasma devices have caught many research interests with the advantages of smaller size, lower power and gas consumption and operation from subatmospheric to atmospheric pressure compared to the traditional plasma devices. In this work, the hollow cathode geometry is adopted in the microplasma devices' design. Different cathode materials, including carbon nanotubes (CNTs) as emitters, are used in the devices. CNTs are known for their excellent field emission characteristics, which makes them a good candidate as the source of seed electrons in the design.

The second device is a pseudospark plasma switch. Pseudospark switches have been applied in pulse power application as the fast closing switches, with hold-off voltage as high as 10 kV. The cathode geometry is hollow, so hollow cathode discharge is formed to increase the charge carrier density. Pseudospark switches need a trigger element where the seed electrons are employed to initiate ionization. In our work, CNTs are used as trigger that supplies the seed electrons.

CNTs used as the electron emitter material are fabricated by chemical vapor deposition (CVD) method. The CNTs are synthesized under different growth conditions, including sputtering time, sputtering pressure, type of catalysts, growth time, and growth temperature. The plasma devices are assembled and tested under subatmospheric pressure in-house in the vacuum chamber. The test experiments are carried out in different background gas, and different operating pressures. Voltage-current characteristics are recorded to study the properties of the plasma. The mathematical simulation are discussed later to study the properties of the plasma in detail.

Acknowledgments

Firstly I would like to express sincere gratitude to my advisor Dr. Hulya Kirkici for the continuous support for my study and research. Her enthusiasm and motivation is always my drive force to search the unknown scientific world. She helped me throughout the research and guided me accomplishing this dissertation. I couldn't have imagined having a better advisor and mentor for me on the seeking path of my PhD degree.

Besides I would like to sincerely thank Dr. Michael Baginski, Dr. Thomas Baginski, and Dr. Wilamoski for the help with review of my dissertation. Thanks for the insightful comments and suggestions. Thank Dr. Blumental from Department of Chemistry for his support and help in the simulation process of plasma and being outsider reader of this dissertation. Thank all the support from the lab mate, Haitao Zhao, Zhenhong Li, Roger Tsai, Ramesh Bokka, Fang Li, Ming Zhang, Baha Yakupoglu, Rujun Bai, Xiangchao Zhu and Michael Jung.

Thank Dr. Wentworth for the opportunity of working in the radio lab and all the fun I had there with the senior students. Thank Ms. Linda Barresi, Mr. Calvin Cutshaw and Mr. Joe Haggerty for mending all the mechanical trouble I have been processed during research. Thank my family and friends for all the support and love.

Table of Contents

List of Tables

List of Figures

Chapter 1

Introduction

Plasma-related industrial processes are becoming popular in practical applications while modern industry is consuming more and more energy nowadays. Plasma is widely used in lighting, fabrication processes, and display area. Therefore, the plasma engineering plays a significant role in increasing the efficiency and effectiveness of major energy-consuming processes applied in industry [1]. Plasma physics and engineering is the interdisciplinary field with the diverse changes in the plasma characteristic parameters. While plasma is in the broad everyday application, the processes inside plasma are complex and complicated. Basic knowledge and the study of plasma properties are still limited in most cases.

One of the major challenges in the plasma applications is that plasma is unpredictable and can easily lead to instabilities and be extinguished. In order to improve these properties of plasma devices, the microplasma is brought out and has attracted more and more research interests recently [2]. The microplasma is referred to as one kind of glow discharge with limited dimensions of 1 mm or less. It is one approach to generate and maintain the stable glow discharge at high operating pressure. Most microplasma are operated from subatmospheric to atmospheric pressures with large number of charged species in a limited space. Therefore, even with the low or moderate ionization degree, the electron density in a microplasma could still reach as high as 10^{15} cm^{-3} [3]. Both the properties and processes in a microplasma are pretty distinct from the traditional glow discharge due to the growth in the surface-to-volume ratio. It has several advantages over the traditional glow discharge, including its small size, high power efficiency, high energetic electron density, low gas consumption, and no requirement of an expensive and bulky vacuum system. Microplasmas usually operate in abnormal-glow mode. This is one of the major challenges of microplasma. Because of this they constantly face the susceptibility of transitioning from the glow discharge to arc. By integrating hollow cathode geometry into the design of the microplasma devices, the microplasma is characterized by both the stable working condition and the high energetic species generated critically in application. As the source of the seed electrons at the initiation stage of breakdown, carbon nanotubes (CNTs) are applied as part of cathode, which are well known for their excellent field emission ability and stable performance with long-hour operation [4].

The other plasma devices introduced in this work is the pseudospark switch design and construction. Pseudospark switch is a three-electrode device similar to the thyratron but operates in low pressure gaseous environment, instead of vacuum. It has a hollow cathode, hollow anode and a trigger. Hollow geometry of anode and cathode is to increase the density of charged species and to confine the plasma. In the modern pulsed power field, the new challenges are presenting as the requirement of high current density and lower jitter time in switch applications. The pseudospark switch is brought up to satisfy such kind of requirements compared to the conventional switches. So far, the pseudospark switch has been designed with the hold-off voltage up to several tens of kV and peak current 10 kA [5]. The triggering mechanism adopted here is field emission triggering with the CNTs as the seed electron source.

The primary objective of this research work is to design and construct two types of plasma devices operating in subatmospheric pressure and apply CNTs as cold cathode material. The design of each device uses easy-to-construct and compact package concept. The performance of each device is represented by voltage-current characteristics. From this, electron density and electron temperature data are extracted and simulated under different operating conditions. The results are presenting to display the optimization working conditions.

Chapter 2

Background Information

2.1 Plasma Engineering

2.1.1 Plasma

Plasma is commonly defined as the fourth fundamental state of matter besides solid, liquid and gas, in which plasma is most energetic state of matter. It is characterized by a mixture of electrons, ions, and neutral particles in which the number of electrons approximately equals to that of ions ($n_e \approx n_i$), whose behavior can be observed in the solid [6], liquid [7] or gas phases. In the following part we refer "plasma" as the gas plasma, which is the focus of our research with no specific instructions. The natural plasmas around us include ionosphere layer surrounding our earth, the aurora, and the lightning bolt in a thunderstorm. The man-produced plasma is widely used in lighting devices with fluorescent lamps and in the sparks in the cylinders of automobile engines in our daily life. Most popular industrial applications of the plasma include plasma spraying, plasma etching in microelectronics, plasma metal cutting and welding, and others.

Different plasmas have variable characteristics in many aspects, including the production methods, the pressure, charged-particle density and temperature. Basically speaking, plasma can be produced by two kinds of methods, assembling the existing constituent particles and ionizing the neutral gas, between which gas ionization is more common method in the applications. The external sources, the presence of external electric and/or magnetic fields, apply to the neutral gas to make sure the particles gain enough energy producing the charged ions and electrons. The initiation of ionization of the neutral gas in the discharge process relies on the energy of free electrons, the number of this kind of electrons and the emission ability of the cathode surface. It has been used widely to produce the plasma with the aid of X-rays, laser beams and high pulse power [8, 9].

2.1.2 Plasma properties

Plasma is denoted as electrical conductor due to the presence of the free charge carriers. The high chemical activity of plasma is also based on the high concentration of active species, mainly electrons existing in the volumetric plasma. Based on the great number of charged energetic particles involved, plasma is considered as an ensemble of complex processes. One region of laboratory plasma interest to us is the positive column of the glow discharge, in which there are equal number of positive ions and electrons. Another region is the negative glow, characterized by high density of ions and highly energetic electrons. Plasma in this dissertation is referred as cold-plasma, where overall charge neutrality exists.

The plasma parameters can span many orders of magnitudes. In most gases, the temperature is one of the critical parameters, which is defined by the average kinetic energy of the particles. Since the plasma is a collection of molecules, atoms, electrons and ions, there are a series of typical temperatures to represent the properties of the plasma. Unless there are sufficient collisions process occurring in the plasma to equilibrate these temperatures, electron temperature (T_e) is usually much higher than the heavy particles' temperature (ion temperature T_i in most cases). Because the mass of an electron is much less than that of a heavy particle, it is going to accumulate energy from electrical field much faster. It is found that the energy difference between electrons and the heavy particles is proportional to the square of the ratio of the energy an electron receiving from the electric field (E) to the pressure (p). Only under small values of E/p, T_i is approaching the level of T_e, which is denoted as thermal plasma or equilibrium plasma, otherwise non-thermal plasma or non-equilibrium plasma. These two different kinds of plasmas have different application areas. Generally speaking thermal plasmas are more powerful, while non-thermal ones are more selective. And thermal plasmas are hard to sustain and manipulate while non-thermal plasmas are more sustainable. Plasma studied in this work are all of the non-thermal kind.

The most common plasma collision processes include ionization of atoms and molecules by electron impact, electron attachment to atoms or molecules, and ion-molecule reactions. Besides these, electron-ion recombination, ion-ion recombination, excitation and dissociation of neutral species by electron impact, relaxation of excited species, electron detachment and destruction of negative ions, photon-release processes also happen in the plasma volume. That explains the case that the processes in plasma are quite complex, combining dozens of chemical reactions of atoms, electrons, and ions and effecting collisions processes all occurring in a very short period of time, creating an operating environment difficult to characterize. There are four basic collision parameters to characterize the processes occurring in the plasma, which are listed in Table 2.1 with the most common representative parameters. The cross section σ of a process is referred as the area around a particle A, in which if the center of another particle B lies in, a collision between particle A and particle B must be in order to occur. Mean free path λ is defined as the average distance travelled by a particle between successive collision processes. The mean free path of a particle A with respect to the collision process with B is related to the cross section of A as follows:

$$\lambda = \frac{1}{n_B \sigma} \tag{2.1}$$

where n_B stands for number density of particle B. The number of collision processes that take place in unit time is called reaction rate γ. It can be expressed as:

$$\gamma = n_B \sigma \upsilon_A \tag{2.2}$$

where υ_A stands for the velocity of particle A. For a two-body collision process A+B, the reaction rate in unit volume can be calculated by multiplying the interaction frequency between particle A and particle B by the number density of particle A, as $n_A n_B \langle \sigma \upsilon_A \rangle$, where the factor $\langle \sigma \upsilon_A \rangle$ is referred as reaction rate coefficient *k*. The reaction rate coefficient *k* is an integral factor as a function of particle's temperature, determined by the particle's energy distribution functions.

Table 2.1 Important parameters to define the collision processes of the particles in the plasma

Collision Parameter	Representative Symbol
Collision Cross Section	σ (cm^2 or Å^2)
Mean Free Path	λ (μm)
Interaction Frequency/ Reaction Rate	γ (s^{-1})
Reaction Rate Coefficient	k (m^{3}s^{-1})

In general, all collision processes can be divided into two categories, elastic collision and inelastic collision. In elastic collisions, there is no net conversion of kinetic energy into other forms. Hence, the total kinetic energy of the system stays constant, only resulting in the kinetic energy scattering. On the other hand, inelastic collisions are more critical for plasma formation. The elementary processes like ionization of atoms and molecules by electron impact are inelastic collisions with the kinetic energy transferred to the internal energy of the particles.

2.1.3 Plasma engineering

Plasma engineering plays a key role in a large variety of industry applications, from microelectronics fabrication and materials processing through environmental utilization and recently cosmetics. It is desirable with the high-energy efficiency, productivity rate and selectivity in the produced plasma. The energetic particles in the plasma are the most important characteristic in plasma application. First, the particles in the plasma usually have higher temperatures and energy density compared to the products of ordinary chemical reactions. The higher energy can be applied to initiate chemical reactions, which are very difficult to start when it used ordinary chemical mechanisms. Second, the energetic particles can generate a wide spectrum of species from electrons, ions, radicals, highly reactive neutral species such as reactive atoms, and reactive molecular fragments, photons, and excited atoms. Despite their extensive usage, understanding of plasma processes in specific system remains limited in many cases. The key point in the application is to find the proper region and optimized plasma parameters among all these varieties in the plasma system to fit the specific usage with peak efficiency. With growing plasma-processing dimensions, the spatial uniformity and the close control in the characteristics of energetic particles are desired in the massive industrial production. The research interests are proposed and focused on the optimized shaped electrodes, multiple generators and different background gas feeding to scale from laboratory reaction to large-area industrial application.

2.2 Subatmospheric Plasmas

2.2.1 Glow discharge

A glow discharge is initiated by the application of a sufficiently high voltage applied between the cathode and the anode. The neutral gas breaks down when the applied electric field reaches to a sufficient amplitude to generate electron-ion pairs by electron impact collisions. The voltage between electrodes at which the breakdown happens is defined as the breakdown voltage V_b. The applied voltage ranging from several hundred of volts to thousands of volts based on the type of gas, pressure, electrode material, the distance between electrodes, and the initial density of free electrons. The presence of an initiating number of free electrons is required to start the ionization process. As Paschen's law states, the breakdown voltage of gas between parallel plates is a function of the product of pressure and gap distance. The equation is shown as:

$$V = \frac{Apd}{\ln(pd) + B} \qquad \text{（2.1）}$$

where V stands for the breakdown voltage in volt, p for the pressure, d for the gap distance between cathode and anode in meter, A and B are constants and depends on the type of the background gas. The typical Paschen curve based on Paschen's law is shown in Figure 2.1. The curve always has a point of minimum voltage to initiate the breakdown, marked as V_{min} in Figure 2.1 for certain value of pd. Based on the location of V_{min} the Paschen curve is divided into left and right side. On the left side of the curve, the breakdown voltage decreases while pd is increasing, which is caused by the rise in the collision frequency between electrons and neutral particles. On the right side of the curve, while collision frequency is too high for electrons to accumulate minimum energy required by ionization process, the ionization cross section is reduced as pd is increasing. As a result of this, the breakdown voltage increases.

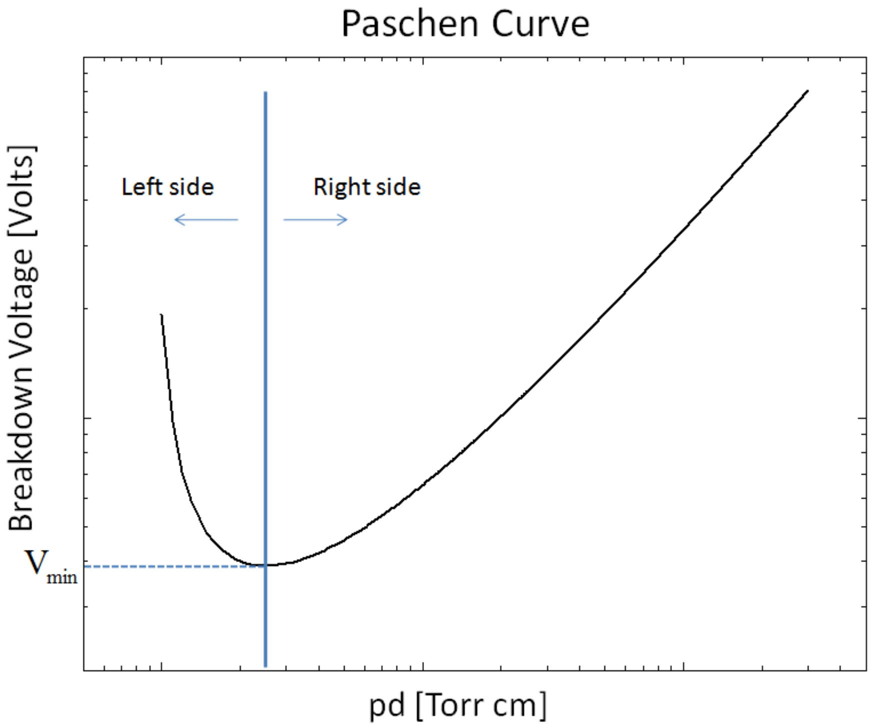

Figure 2.1 Typical Paschen curve for breakdown voltage versus the pressure-gap product

Glow discharge is the base form of fluorescent lighting. Basically speaking, when the pressure is around several Torr, or the operating circuit has a ballast resistor to prohibit a large current flow, the glow discharge is developed. From macro perspective, it is a kind of weakly ionized plasma with low current and high voltage. Normal glow discharge is defined as the plasma produced after breakdown where as current increases the sustaining voltage remains constant. This means that the current density in the boundary region is constant. The cross-sectional area of the discharge increases and is proportional to the current. As long as the discharge area is less than the area of the cathode, this V-I characteristic remains the same. Once the discharge covers the electrodes completely, any increases in discharge current would lead to an increase in the discharge voltage, with the current density increasing. This type of increasing V-I characteristic shows a positive resistive property, denoted as "abnormal glow discharge" mode. This mode is applied mostly in the atomic spectroscopy measurement because of large amounts of excited species and particles. With the increasing current, the discharge would lead to a transition to the arc discharge with instability. Another situation similar to the current raising is increasing the pressure. Under the same current condition, the current density is proportional to the square of the pressure [10]. There is a current density threshold to develop this glow-to-arc transition as the pressure increases. The value of this current density threshold is determined by the operating characteristics, including the gas type and electrode material. For example, if the pressure is on the order of an atmosphere with the low external circuit resistance a thermal arc discharge may come with large currents around 1 A after abnormal glow discharge mode.

Most of the plasma produced by the glow discharge is nonequilibrium plasma, which means electrons have higher kinetic energy than the ions and neutral particles. The population of the various excited species is determined by the electron energy distribution function. Generally speaking, the relative distribution of the various plasma particles can be manipulated by simply changing the electron energy distribution. This nonequilibrium plasma has been applied in many applications based on the high electron energy distribution function [11].

In order to maintain a stable glow discharge, the control needs to be applied to make sure the current density is below the transition threshold. The most common and easiest way is to adapt current-limiting resistor in the discharge circuit. Glow discharge devices are gaseous conductors with inert gases (mostly argon and helium) operated from subatmospheric to atmospheric pressure. They are basis of fluorescent lighting in everyday life, with mercury vapor and neon as the discharge gas vapors. In power electronics industry, the pseudospark switch as cold-cathode thyratron and ignitron are developed utilizing glow discharge as the switching and rectification medium. Furthermore, the glow discharge devices have the compatibility with solid elemental analysis and depth-resolved analyses using excited atoms and ions. By the interaction of external light sources, glow discharge devices could be used in atomic fluorescence, optogalvanic effect, and resonance ionization spectroscopy.

2.2.2 Hollow cathode discharge

Hollow cathode discharge is referred as the gas discharges generated by a hollow-structural cathode and an arbitrarily shaped anode. The concept of hollow cathode discharge was firstly brought up by A. D. White in 1959 [12]. The most common cathode structure in the hollow cathode discharge has a cylindrical hole in the center and is separated from the ring-shaped anode or the metal-needle anode with a dielectric spacer [13]. It has the advantages of the high electron density and low-pressure working range. It is known that the non-plane cathode geometry affects the discharge distribution dramatically. In a broad sense hollow cathode discharge is referred as all glow discharges generated by non-planar cathodes [14]. It has a wide range of applications, including hollow-cathode lamp, hollow-cathode laser, and hollow-cathode plasma switch.

In addition to the well-known scaling parameter of pd in the Paschen's law to determine the breakdown voltage in a glow discharge, the hollow cathode discharge has another unique scaling parameter referred as pD, in which D stands for the dimension of the cathode aperture. In most of cases when the cathode has a cylindrical hole, D stands for the diameter of the center hole. According to Allis-White similarity law, the pressure p varies inversely with the diameter of the hole D [15]. The range of pD determines the voltage-current (V-I) characteristic in the hollow cathode discharge. In order to operate the hollow cathode discharge with stability, pD needs to be in the range between 0.1 Torr • cm and 10 Torr • cm under the constant sustaining voltage V_s [16]. The lower boundary of pD is determined by the condition that the diameter D must be greater than the mean free path for ionization, while the higher boundary depends on the condition that the distance between opposite cathodes must not exceed the lengths of the two cathode fall regions. Hence, for atmospheric pressure operation the diameter of the cathode hole should be in the order of 100 μm [11].

Due to the hollow geometry, the dimension of the cathode aperture D controls the width of the dark space. When reducing D to a sufficiently small level, it leads to the merger between cathode negative glow and anode glow as well as rise in both light emission and cathode current density. It is commonly referred as hollow cathode effect [17], which has been proved caused by pendulur electrons [18]. The free electrons emitted from the trigger unit are accelerated and propagates in the cathode cavity. Once the breakdown occurs further electrons are generated. These electrons are in the field free region of the cathode cavity and reflected back and forth between the boundaries of the cathode cavity. This results in the increase of ionization and formation of high energy density and number density of charged species (Figure 2.2). The hollow cathode discharge is also a kind of a nonequilibrium plasmas, in which the ions and neutrals have a much lower temperature compared to the electrons. The simulation results of direct-current microhollow cathode discharge with 200 μm opening show that the peak electron temperature reaches tens of eV while the peak gas temperature stays around several hundreds of Kelvin [19]. Therefore, the high-mobility electrons move faster in the reverse direction of electrical field and leave the low-mobility ions behind, forming a virtual anode in the cathode cavity. The existence of the virtual anode in the cavity further increases the electron emission rate.

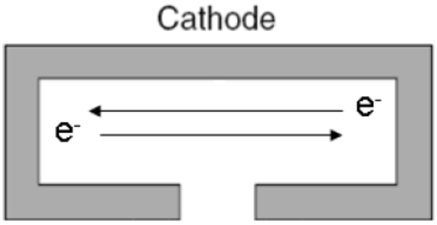

Figure 2.2 Schematic movements of the pendulur electrons in the cathode cavity

2.2.3 Microplasma

Microplasma is defined as plasma, which is spatially confined to 1 mm or less. It is one approach to generate and maintain the stability of the glow discharge at subatmospheric or atmospheric pressure [2]. The physical and chemical properties differ from large-scale plasmas due to the increase of the surface-to-volume ratio. To make sure the proper multiplication rate of free electrons in the limited distance between cathode and anode, higher operating pressures are mostly adopted to assure high-density particles. Hence, even with the moderate ionization degree, the electron density existing in microplasma can reach as high as 10^{15} cm^{-3} [20]. Nowadays, microplasma can be found in many applications, mainly taking advantages of the low power consumption, the small size, the non-thermal characteristics, and the simple operation ranging from subatmospheric to atmospheric pressures. In addition to the high electron density in microplasma discharge, the electrons have the non-Maxwell electron energy. There are many microplasma devices with different geometric configurations, including pin electrodes, parallel-plate electrodes, hollow cathodes, and inverted-pyramidal electrodes [21-24]. In a previous work, it has been utilized in display systems by studying the electrostatic breakdown in vacuum-packaged microelectromechanical system (MEMS) with the volume confined by magnets [25]. Microplasma devices have also been employed as the detector according to the spectral information. For example the water sample can be placed as a cathode in order to identify the impurities in water [26]. The parallel-plate electrodes with multiple 1.5 mm-diameter holes are studied to decompose the pollutants of NO_x in exhaust gas [27]. The silicon deposition at elevated pressure and room temperature are reported using plasma-enhanced chemical vapor deposition method with DC microplasma [28]. It is reported that the surface of polyethylene naphthalene film can be treated by the microplasma produced by the Marx generator to modify the surface wettability, with the advantages of environmental-friendly characteristic and low cost [29]. High-pressure discharge in xenon was found to be a strong source of excimer radiation, utilizing 100 μm-diameter opening hollow cathode discharge with DC voltage 220V [30]. Generally, the power of a microplasma is limited that the individual microplasma discharge has limited applications. Hence, most industrial applications require microplasma arrays or microplasma integrated structures to boost the processing power. In order for a stable operation of multi-microplasma discharge in parallel, a positive differential resistance characteristic is desired to avoid the employment of the extra ballast resistors in the operating circuits.

As Paschen's law indicates, the minimum breakdown voltage occurs when the product of pressure and the gap distance is around the level of 0.1-5 Torr • cm for most common gases [31]. When the pressure increases, the inter-electrode distance needs to be decreased to maintain the same breakdown voltage. Consequently, when the inter-electrode distance lies in the order of micrometers, the operating pressure of a glow discharge can be as high as or higher than the atmospheric pressure under constant breakdown voltage. After the breakdown happens, multiple collision processes between variety particles would produce more charged species with a proper voltage V_s applied, which is known as sustaining voltage, lower than the breakdown voltage V_b usually.

Under the atmospheric pressure, the nonequilibrium plasma is susceptible to glow-to-arc transition since the product of pd increases, which leads to instability because of the high current density. One method to eliminate this kind of instability is to confine the plasma to dimensions of 1 mm or less to make sure the product of pd falls in the area of normal glow discharge without changing the breakdown voltage in general. Besides, the large surface-to-volume ratio in the microplasma boosts the energy losses of the charged and radical particles in the boundary, which would prevent the run-away transition to an arcing mode. This makes the gas temperatures in the microplasma, typically hundreds of Kelvin above room temperature, are much larger than most low-pressure glow discharges [32].

The most common studies of microplasma are divided into two categories namely experimental techniques and numerical techniques. These are consistent with the acknowledge methods of the normal plasma however with much more complexity due to the limited volume in the microplasma.

Microplasma with hollow cathode geometry is referred as the gas discharges between a hollow cathode and an arbitrary shape anode with the dimensions around 100 μm range. It works similarly to the conventional hollow cathode discharge to produce high-density electrons. As pD lays in the range of 0.1 Torr • cm and 10 Torr • cm, as mentioned before in the hollow cathode discharge, the microplasma with hollow cathode construction develops in stages, from pre-discharge at low currents to hollow cathode discharge at high currents. It has been reported that the large concentration of electrons with high energy favors excimer formation at wavelengths of 128 and 172 nm in xenon and argon respectively [33].

2.2.4 Pseudospark switch

A pulsed power system has the main characteristic of very high peak-to-average power ratio of the electric pulse(s). The basic working principle of a pulsed power system is to accumulate energy for a relatively long period of time (usually seconds or minutes) and then to release or discharge it to a load over a much shorter period of time (usually microseconds or nanoseconds). In general, a pulsed power system consists of an energy storage stage, a pulse forming stage, a switch and a load [34]. The properties of the switches are critical to the pulsed power system, affecting the rise time, pulse shape and the amplitude of the output pulse.

The pseudospark switch, also known as cold-cathode thyratron, is designed like thyratron to control high voltage and high current discharges and operates at low pressure. The development in pulsed power system has exceeded the capabilities of the common commercial switches such as thyratron or spark gaps recently. To meet the new requirements, the pseudospark switch has been brought up by Christiansen and Schultheiss in 1978 as low-pressure, high-voltage plasma devices [35]. Compared to other switches, the pseudospark switch is capable of high speed switching, high lifetime, and high current rise of about 10^{12} A/sec. Due to the symmetric design of the electrodes, pseudospark switch has the ability to handle 100% reverse current without failure. It has been widely used in pulsed power systems, linear accelerators, material processing devices to produce intense pulsed electron beams, soft x-ray source, and high power excimer laser [36-40]. Besides, the pseudospark switch has the advantage of easy-construction and is free of electrode erosion. The hold-off voltage of a single gas pseudospark switch depends significantly on the surface flashover and the field emission of the cold cathode. In general, the hold-off voltage in the switch design can be increased by adopting multi-gap switch configuration or filling gases of hydrogen, helium and other inert gases. An upgraded double-gap pseudospark switch has been designed and tested with the hold-off voltage as high as 40 kV and peaks current 5 kA [41]. Pseudospark switches make use of hollow cathode geometry, taking advantage of the hollow cathode effect. The general construction of a pseudospark switch is shown as Figure 2.3. The switch consists of a hollow cathode and a hollow anode, which has one or several holes (2 holes in the picture) in the interface to produce the spark in the operation. It is verified that the inter-electrode distance needs to be designed as comparable as the hollow diameter for the purpose of high-current discharge [36]. In the cathode cavity, the trigger unit is placed to initiate breakdown between the cathode and the anode. Most of the trigger methods include the electron injection, the plasma injection, optical triggering and the surface discharge.

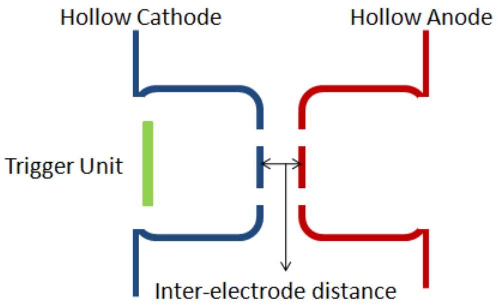

Figure 2.3 General construction of pseudospark switch

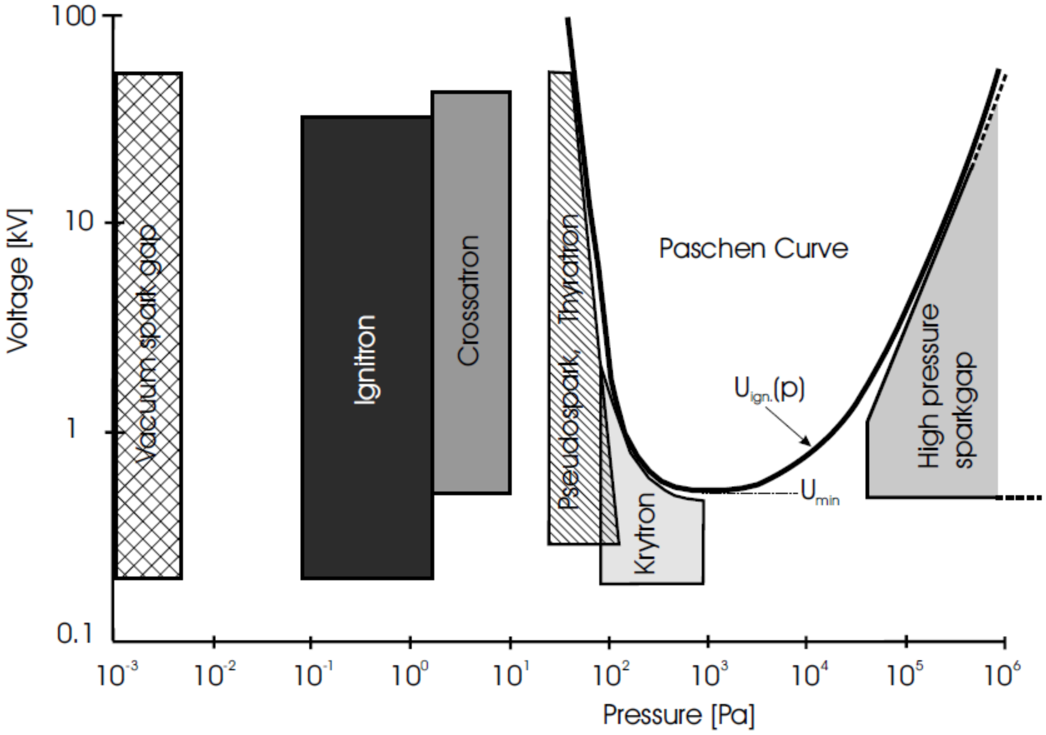

Figure 2.4 Range of gas pressures and operating voltages for various types of gas switches (inter-electrodes distance=3 mm) [34]

A pseudospark is a high voltage discharge with the product of the inter-electrodes distance and the operating pressure located on the left side of the Paschen's curve (Figure 2.4). Generally, the pseudospark discharge process is summarized into four phases, including predischarge, hollow cathode discharge, super glow discharge and decay of the discharge plasma [42]. At low currents, predischarge phase is observed with glow discharge with the cathode fall occurring outside the hollow cathode structure. As the current increases and the glow discharge transition into the abnormal discharge with a positive differential resistance, the positive space charge region relocates closer to the hollow cathode structure until entering the cavity. A virtual anode is formed in the cavity and results in redistribution of the electric field, as the hollow cathode effect arises.

In this transition from the axial pre-discharge to a radial discharge, a negative differential resistance is observed in the current-voltage characteristic, which is normally referred as hollow cathode discharge. The continuous transition develops into high-current-density discharge phase, referred as "super glow discharge", and characterized by a positive differential resistance. It is often accompanied by the production of intense electron beam from the central hole in anode. The electron beam power densities have been reported as high as 10^9 W/cm^2 with corresponding current density as 7×10^4 A/cm^2 and applied voltage as 20 kV [43]. When the time interval of the pulse power exceeds certain time limit, the recombination and diffusion movements of the residual charged particles in the hollow construction would become dominate, resulting in the decay of discharge plasma. The minimum time limit, referred as recovery time for a pseudospark device, has been investigated as the function of hollow cathode length and radius of gas volume [41].

2.3 Limitations of Subatmospheric Plasmas

2.3.1 Lifetime limits

The basic idea about the plasma application is to transfer the energy into producing energetic particles and get processing with a different medium in practice. Although the energetic particles existing in the plasma are one of the advantages in the plasma applications, they still cause problems such as the electrodes erosion at high currents condition. It is the same case as the main drawback in thermal plasma applications. High energetic particles in thermal plasma normally cause overheating problems of reaction media and result in the short lifetime of the plasma devices. It has been shown that the face of the cooper cathode can be evaporated due to the high power density of the electron beam (10^9-10^{12} W/cm^3), leading to rapid electrode degradation [44]. Changing the electrode material to higher-temperature material is the most common way to reduce the electrode erosion and increase the lifetime of the plasma devices. Besides, the optimization of applied magnetic field design is performed to increase the lifetime [45]. Changing geometry design of plasma devices could be another approach to solve the lifetime limitation. The Jet Propulsion Laboratory (JPL) scientists and engineers developed a sophisticated hollow cathode design, which was able to work continuously for 30,352 h with high discharge current 4~15 A [46].

Besides, another approach is to develop methods for precise control of the flux and energy of the reactive species through transferring stable energy over long periods. This is specifically required when applying plasma source on delicate materials such as living biological organisms in cosmetics [47]. The key of this method is to develop real-time diagnostic technology and eventually autonomously controlled plasma equipment with active feedback.

2.3.2 Electron density limits

In pseudospark switch application, one of the major problems is current quenching [48]. It happens because of the depletion of charge carriers in the high current conduction phase, caused by the interaction of plasma and cathode surface [46].

A popular method is to reduce the current quenching to an allowable level by increasing the gas pressure, which introduces the additional particles in turn. Besides, it could be suppressed by optimizing the electrode geometry, by the addition of heavier gases and by applying long pulse trigger voltage.

The ability of the trigger unit to deliver a sufficient number of electrons into the cathode cavity is critical for a reliable triggering and limited delay time in pseudospark switch. The higher electron injecting number in the same time frame it supplies, the lower delay time the pseudospark switch can achieve. As a trigger unit in pseudospark switch, it is necessary to provide at least 10^9 electrons to ignite the discharge [49].

2.3.3 Power consumption limits

Generally speaking, the plasma reactor always desires high operating power to maintain the operation. As power consumption concerns, most plasma devices are still on the transition from research laboratory to industrial-scale applications. For example, plasma CO_2 dissociation attracts researchers' interest to reverse climate changes while the bottleneck is the limited energy transfer efficiency [50].

Power efficiency has been a paramount concern in industrial applications. Study on subatmospheric plasma devices has brought a series of methods to boost the power efficiency, including experimental and simulation approach. For example, a two-dimensional fluid model is brought up to investigate the power efficiency as a function of applied electric field in the plasma display panel cell with continuous electron beam source. The power efficiency can be enhanced by reducing the electric field inside the cell to boost the number density of the excimer species [51].

Chapter 3

Carbon Nanotubes

3.1 Introduction

In order to improve the performance of the microplasma and pseudospark device, a proper cold cathode emitter material is needed to supply seed electrons to initiate the plasma. Ideally, the cold cathode is desired to have a high field emission capability. As Table 3.1 shown, different materials have been studied and the results of the turn-on field and the saturation current density are reported in several papers [52-55]. The turn-on field varied from 0.43 V/µm to 6 V/µm, while the saturation current density from 0.4 mA/cm^2 to 1 mA/cm^2. It is conducted that CNTs have the lowest turn-on field and satisfied saturation current density compared to Cu_2S nanowire, polycrystalline diamond and ZnO nanowire. These two characteristics make CNTs a good candidate for cold cathode emitter material.

Table 3.1 Turn-on field and saturation current density of typical electron emitter materials

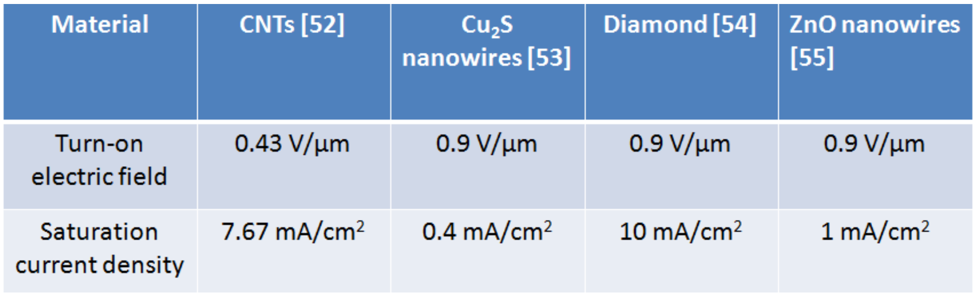

Material	CNTs [52]	Cu_2S nanowires [53]	Diamond [54]	ZnO nanowires [55]
Turn-on electric field	0.43 V/µm	0.9 V/µm	0.9 V/µm	0.9 V/µm
Saturation current density	7.67 mA/cm^2	0.4 mA/cm^2	10 mA/cm^2	1 mA/cm^2

Carbon nanotubes (CNTs), first produced by arc discharge [55], are the most promising nano-scale material for its excellent electrical, thermal, and mechanical properties. CNTs have high aspect ratios in the form of tubes with the diameter in the order of several nanometers and the length in the order of several micrometers. They are known for the characteristics of great electrical conductivity, high mechanical strength, and high resistance to chemical and physical attacks. Besides they are also known for their excellent field emission characteristics due to their high aspect ratio, which makes them a candidate of the cold cathode material in high-power applications [56]. It has been reported that with the applied voltage 200 volts, the field emission current density could reach as high as 0.1 mA/cm^2 [57]. The high conductivity is confirmed with resistivity of 0.1 Ω·cm in the highly-dense aligned CNTs arrays [58]. These remarkable electrical properties of CNTs make them a potential material in the microelectronics application and other areas such as high performance field-effect transistors, single-electron transistors, atomic force microscope tips, field emitters, and chemical/biochemical sensors [59]. Digital circuits based on transistors fabricated from

CNTs have been reported by M. M. Shulaker group to potentially further reduce the size of electronic devices made by Si with improved energy efficiency [60].

Most of CNTs are classified into two categories of Single-Wall Carbon Nanotubes (SWCNTs) and Multiwall Carbon Nanotubes (MWCNTs). SWCNTs can be considered as the formation of a graphene sheet rolled up as shown in Figure 3.1(a). MWCNTs are a group of concentric SWCNTs with different diameters of tubes as shown in Figure 3.1 (b). From the view of the orientation point in the nanotubes, CNTs can also be classified into vertically aligned CNTs and randomly aligned CNTs as shown in Figure 3.2. The orientation points in aligned CNTs are all in one direction. Compared to random CNTs, the tube density is much higher in aligned CNTs. By altering the catalyst species, both kinds of CNTs can be easily produced by chemical vapor deposition method in this work.

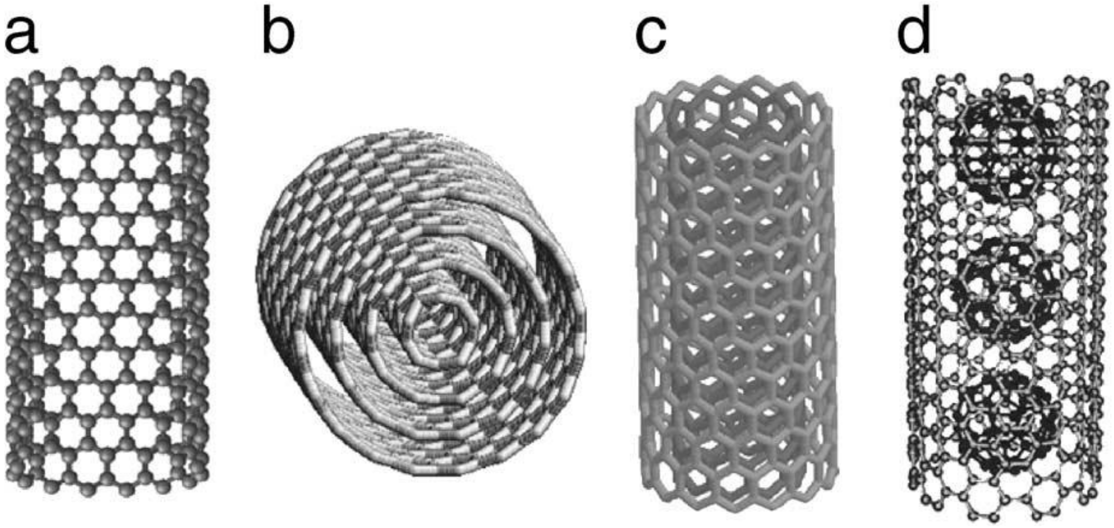

Figure 3.1 Schematic diagram of (a) a single-wall carbon nanotube (SWNT), (b) a multi-wall carbon nanotube (MWNT), (c) a double wall carbon nanotube (DWNT) and (d) a peapod nanotube consisting of a SWNT filled with Fullerenes (e.g., C60) [61]

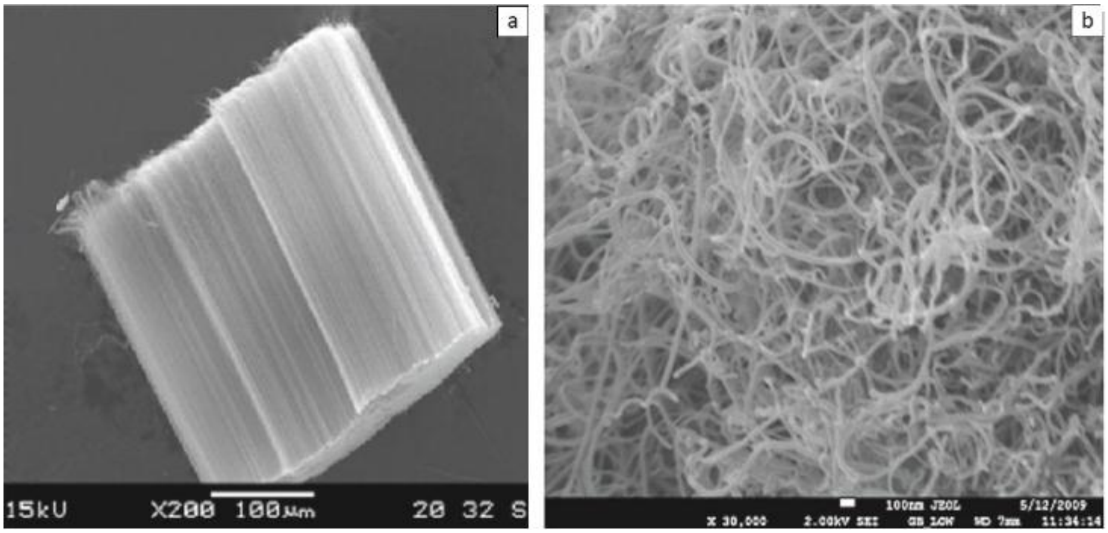

Figure 3.2 SEM pictures of (a) aligned CNTs, (b) random CNTs [62]

The CNTs can be obtained using high-pressure arcs [63], laser ablation [64], chemical vapor deposition (CVD) [65], and plasma torch [66]. The properties of the CNTs are determined by the structures of nanotubes, including the diameters and lengths. The growth conditions are studied broadly to control the growth rate, the diameter, the length and the areal density of the nanotubes in CNTs. In the plasma enhanced CVD (PECVD) method, it has been reported that the properties of the produced CNTs are a function of the catalyst layer thickness, electric field strength, deposition temperature, feeding gas flow rate, and pressure [67].

In this research, electron sources are critical to determine the performance of microplasma device and pseudospark switch. The cold electron emitter material as CNTs is applied as an improvement over the conventional thermal electron emitter material. As thermal electron emitter material, one of the dominant disadvantages is that the emitted current density is limited by the thermionic emission properties of material itself. Another concern is thermal instability and thermal expansion in the material. The cold electron emitters are attracting more and more interests for showing great potential to overcome these disadvantages in a series of applications.

Field emission implies extracting seed electrons from a solid surface by tunneling through the surface potential barrier. The current density of the field emitter is a function of the local electric field and the work function at the emitting surface. CNTs have the ability to sustain the large current densities for a considerable time range without obvious deterioration [4]. The development of CNTs research shows that nanotubes can be planted directly onto the desired substrates with satisfied conductivity over a large area. The first stage of the project is to optimize the properties of synthesized CNTs to achieve the goal of applying them as electron emitter source in the devices.

3.2 Properties of CNTs

CNTs have a series of properties including excellent thermal conductivity and varying electronic properties based on their aspect ratio. For example, by introducing CNTs into synthesizing novel polymer compounds, the material can shield the electromagnetic interference [68]. The properties of CNTs are classified into electrical property, chemical property and mechanical property as discussed below.

3.2.1 Electrical properties

It has been shown that electronic properties of CNTs are strongly modulated by small structural variations [69]. Based on the diameter and the helicity of atoms in the nanotube shell of CNTs, they can be either metallic or semiconductor. Applying four-point probe method, it has shown that the resistivity of MWCNTs ranges from 5.1×10^{-6} to 1.2×10^{-4} Ω•cm, while SWCNTs ranges from 3.4×10^{-7} to 1.0×10^{-6} Ω•cm [70, 71]. The resistivity of MWCNTs is larger because of less conductivity between the multi-layers only located in MWCNTs. It has been observed that both metallic and non-metallic behaviors are presented in SWCNTs by varying temperature [72]. Besides, chemical treatments have been found to affect the conductivities of CNT fibers significantly. Oxidizing the CNT fibers in air or HNO_3 would increase the conductivity and change the conduction behavior [73]. These all indicate that the resistivity of CNTs varies by orders of magnitude and have a far wide range of electronic conductivity.

The metallic CNTs are used in interconnection of Very-Large-Scale Integration (VLSI) circuits because of low resistivity and mechanical stability [74]. The SWCNTs array is reported with current density as high as 10^9 A/cm^2 without any heat sink. Compared to Au-nanowires, CNTs have higher current carrying capacity and larger thermal conductivity, which demonstrates the potentials of CNTs to provide a solution for demanding requirements of high current densities and endurance in VLSI industry. With the low turn-on voltage in field emission test, they are ideal candidate as the material of flat-panel displays. CNTs supercapacitors are studied because of better electrical and mechanical stability compared to other capacitor materials [75]. The high surface-to-diameter ratio gives CNTs the ability to store energy along the tubes.

3.2.2 Chemical properties

CNTs' cylindrical nanostructure makes it ideal candidate in many chemical and biological applications based on their high surface-to-diameter ratio. They are highly graphitized carbonaceous materials with low chemical reactivity. The oxidation of CNTs needs reaction temperature higher than 750 ℃, which could increase chemical reactivity and modify the chemical properties of CNTs [76]. When it comes to composite material fabrication, the oxidation of CNTs is most employed to enhance the purity and modify the chemical inertness achieved by oxygen plasma treatment, wet chemical reactions and photon oxidation. Besides, it is found out that CNTs with defects in construction or mixed with alkali metals are more vulnerable to chemical reactions [77]. After the oxygen-interfacial-adhesion treatment, CNT-based composites could perform the excellent electrical and mechanical properties of CNTs. Many studies have been carried out applying CNTs in electrochemical biosensors, based on their high surface-to-diameter ratio and excellent conductivities. Absorption properties of CNTs make them qualify as membranes to filter toxic chemicals, dissolved salts and biological contaminant from water [78]. Application of CNTs as polyvalent tools in cancer treatment is promising as the targeted drug delivery [79]. The construction of CNTs allows them penetrate cells and deliver drug to cancer or knock off the unwanted genes. They have high drug loading capacities because of high aspect ratio.

3.2.3 Mechanical properties

CNTs are considered as the strongest and stiffest material discovered so far both as in tensile strength and elastic modulus respectively. SWCNTs have been tested with tensile strength of 100-150 GPa as in the Young's modulus. They are verified with very high stiffness to an axial load, depending on helical formation and temperature [80]. According to the tensile-loading experiment, the outermost layer of individual MWCNTs performs tensile strength of 270-950 GPa in axial direction as in the Young's modulus [81].

Based on their excellent tensile strength and light density CNTs have been studied to create artificial muscles. CNT aerogel has been constructed and used to convert electricity into chemical energy as soft muscle does. It has ability to retain the shape after thousands of times' compression and be operated under extreme conditions [82].

3.3 CNTs Fabrication and Optimization

There are a series of methods to synthesize CNTs. The most popular methods nowadays include arc discharge [63], laser ablation [64], chemical vapor deposition (CVD) [65] and plasma torch [66]. Among these methods, plasma enhanced chemical vapor deposition (PECVD), which falls into the CVD category, is the most commonly used one because of simple equipment required and excellent uniformity when it comes to the deposition over large area. Generally speaking, the growth of CNTs is the process of decomposing hydrocarbon gas mixture and regrouping the carbon atoms into the tubes shape. There are two main proposed growth mechanism, tip-growth and base-growth, based on the metal particle position in the synthesized CNTs [83]. In tip-growth, the metal catalyst particles would lift off from the substrate and remain at the top of the CNTs; while in base-growth, the catalyst remain anchored to the substrate. In both cases, CNTs' growth only happens at the site of the metal catalyst particles.

In this work, CNTs are synthesized using CVD method with metal catalysts sputtering first. Silicon wafer are prepared at the very first stage of the fabrication as the substrate. The physical vapor sputtering (PVD) is applied to coat the metal catalyst on the silicon substrate. Then the CNTs are synthesized in a CVD furnace with the gas mixture of acetylene (C_2H_2) and argon (Ar). Scanning electron microscopy (SEM) and field emission test are employed in the work to characterize the properties of the CNTs. The synthesis conditions, including catalyst types and thickness, gas flow rate and furnace temperature, are investigated to optimize the outcomes of CNTs. Both randomly and vertically oriented CNTs are tested and presented. The substrate of Si is pre-treated by applying basic photolithography technique to confine the distribution of the metal catalyst particles to produce selectively growth of CNTs.

3.3.1 Silicon wafer preparation

The plain Si <100> n-type wafers are cleaned according to the standard Radio Corporation of America (RCA) cleaning procedure. The process is carried out in Alabama Micro/Nano Science and Technology Center (AMNSTC). The cleaning process is designed to remove organic contaminants, thin oxide layer and ionic contamination for preparation of high-temperature processes. Then, a 20-min dehydration bake step is performed in vacuum chamber to remove moistures, which may compromise the adhesion between silicon and the sputtering catalyst.

In order to grow CNTs selectively from specific sites on substrate, Si wafer is pre-treated by basic photolithography technology to have patterned catalyst arrays showed as Figure 3.3. 5-min hexamethyldishilazane (HMDS) treatment is applied as the first step to improve the adhesion between Si wafer and photoresist (PR). The negative tone lift-off PR of AZ®-nLoF 2035 and the AZ®300 MIF positive photoresist developer are adopted based on the mask's pattern. The developing process of the substrate in detail is listed as following:

Step 1. Coated with PR at a speed of 2000 RPM for 20 seconds;

Step 2. Soft-baked on a hot plate at 110 ℃ for 90 seconds;

Step 3. Exposed to a radiation (193 nm UV light) source for 20 seconds;

Step 4. Post-Exposure baked on a hot plate at 110 ℃ for 90 seconds;

Step 5. Developed with AZ®300 MIF for ~ 2 minutes.

After the pre-treatment of photolithography, the substrate is transferred into Physical Vapor Deposition (PVD) chamber for a thin-film deposition of metal catalyst. The detail is introduced in the following section. After the deposition of the catalyst, the substrate is dipped into acetone for a couple of minutes to remove unnecessary PR along with iron catalyst on top. That is the patterned substrate successfully prepared for selectively growth of CNTs.

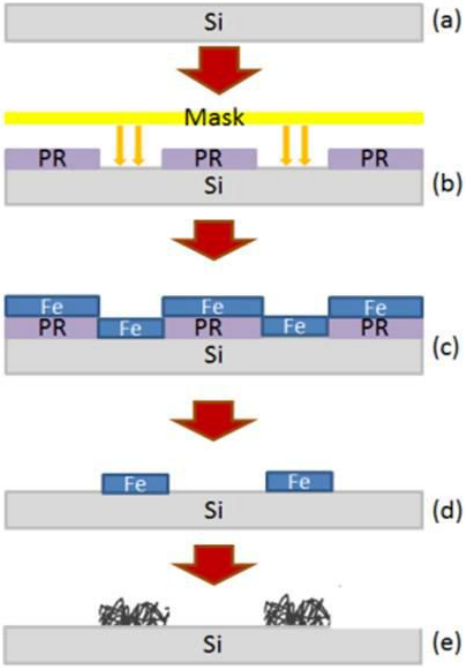

Figure 3.3 Schematic diagram of CNTs fabrication processing (a) silicon wafer cleaned and baked; (b) patterned photoresist removed by aligned mask for deposition of iron catalyst; (c) iron catalyst sputtered; (d) photoresist removed along with the iron catalyst on the top; (e) CNTs selectively grown on the substrate in CVD furnace [84]

3.3.2 Catalyst PVD

Physical vapor deposition (PVD), also known as sputtering deposition, is a method for depositing thin metal layers on semiconductor wafers by vaporization of the target material in industry. The PVD processes are classified as DC sputtering, radio frequency (RF) sputtering, magnetron sputtering, and reactive sputtering. PVD can process different compounds, including metals, alloys, and dielectrics while applying different power supply. The sputtering target provides the PVD system a stable, long-lifetime vaporization source. The sputtering yield is controllable by adjusting the feed gas flow, the power supply and the coupling angle between the source and the substrate. The working condition needs carefully observation since most PVD systems are operated under high vacuum and high temperature. The cooling system is necessary for the long-lifetime target utility.

After the wafer preparation process, the wafer is loaded into a DC/RF PVD chamber with 2-inch magnetron sputtering system. The plasma gun is located 15 cm straightly under the mounted wafer. The plasma source in the chamber is glow discharge without filament, produced based on the principle of microwave plasma discharge. A 2-inch-diameter iron target is employed as the source of the catalyst particles. It is located on the top of the plasma gun. With the ion bombardment activities produced by the plasma, catalyst particles would gain enough energy to break off the bound and get free to attach the wafer ahead. The chamber is pumped down by both the mechanical and turbo pump to the level of 10^{-6} Torr and then argon is fed as the breakdown gas. 7-milliTorr-pressure is maintained during the whole PVD process.

Annealing is done after the catalyst sputtered, which transfers the thin film catalyst layer into nano-scale seeding sites or islands due to different thermal expansion coefficients for the substrate and the catalyst. The size of the islands are determined by the thickness of the sputtered catalyst.

3.3.3 CVD method

Chemical Vapor Deposition (CVD) is a widely adopted method to synthesize CNTs and has the advantages of easy-to-construct, low-cost and controllable growing conditions over other methods. The process happening in the CVD is considered as the carbonaceous gas, such as methane, and the feeding gas are thermally decomposed on the surface of the catalyst particles. While the carbon compound attaches to the catalyst, the rest of the by-products is carried away by the gas flow. In the tip-growth mechanism, the dissolved carbon would diffuse through the catalyst particles from the surface to the substrate and form the nanotubes on the bottom of the catalyst layer. In the base-growth mechanism, the carbon species with the rapid diffusion coefficient would go through the catalyst from the bottom, resulting in the catalyst particles remaining at the bottom of the nanotubes.

The CVD chamber consist of a quartz tube (Figure 3.4). A resistive heater is applied to heat the chamber and chamber temperature is monitored closely. Mixture of Acetylene (C_2H_2) and Argon (Ar) with flow rate of 20 sccm and 75 sccm respectively is feed into the chamber. Flow and pressure in the chamber are controlled by the flow meter and a set of valves. The reaction pressure of 70 Torr is maintained. The growth temperature is kept at 700 ℃ and the growth time is varied from 10~240 min with different outcome CNTs.

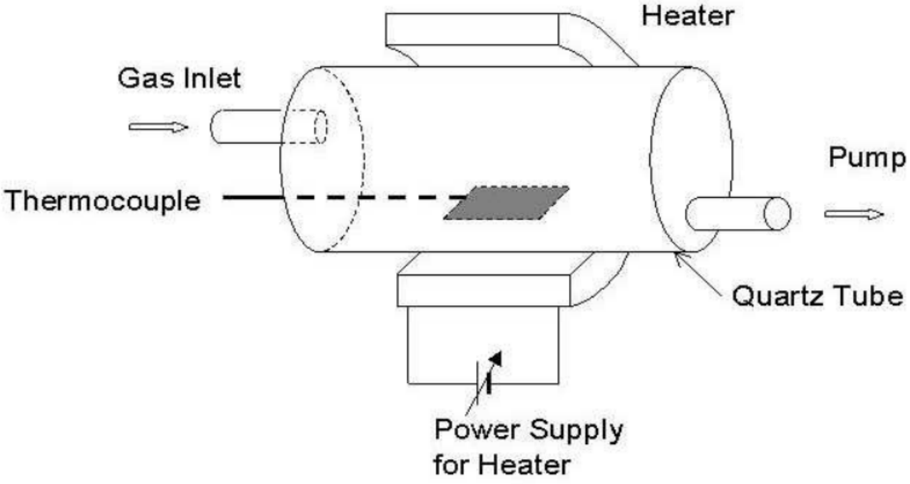

Figure 3.4 Schematic of CVD reactor [85]

3.3.4 Examination methods

To evaluate the electronic and mechanical properties of CNTs, different examination methods are used, including tensile-loading experiment, Raman spectroscopy, X-ray Photoemission Spectroscopy (XPS) and Scanning Electron Microscopy (SEM). SEM is employed in this work to produce the image of synthesized CNTs.

Electron field emission is the concept of electrons emission by applying a strong electric field on a solid material. This experiment is usually carried out in vacuum. The emission current consisting of the extracted electrons tunneling through the surface potential barrier by the effect of the strong electrical field is used to characterize the electrical ability of the solid material. In this research, the number density of the seed electrons introduced by CNTs is one of the critical parameters to boost the efficiency of the microplasma devices and pseudospark switch. Therefore, in order to optimize the design, higher electron field emission is considered necessary. Once the synthesis of CNTs is completed, the sample is transferred into vacuum chamber to finish the electron field emission test to represent the electron emitter ability.

3.3.5 Results and discussion

According to the research, the growth conditions of the CNTs determine the density, diameter and length of the nanotubes. The reaction temperature of the CVD chamber, the flow ratio of C_2H_2 concentration and the sputtering time (thickness of the catalyst) are studied in the earlier work [62].

In order for the convenient integration of CNTs sample with circuit, patterned CNTs are introduced with the process shown as Figure 3.3. The pattern shape is designed as square with different gap size, listed in Table 3.2 with detailed dimensions. The selective mask is shown in Figure 3.5 (higher-left), with each pattern type in one quarter. After the photolithography process the wafer is shown in Figure 3.5 (lower-right) and ready to transfer into PVD chamber for the catalyst sputtering. The PR is acting as the barrier to prevent catalyst attached to SiO_2 under-layer. The processed wafer under microscope using the same magnifying power is shown in Figure 3.6, labeled by the corresponding pattern marker listed in Table 3.2.

Table 3.2 List of pattern size in the selective mask (one form of pattern for each quarter)

Pattern marker	Size	Gap
A	25 µm x 25 µm	25 µm
B	25 µm x 25 µm	50 µm
C	25 µm x 25 µm	100 µm
D	50 µm x 50 µm	25 µm

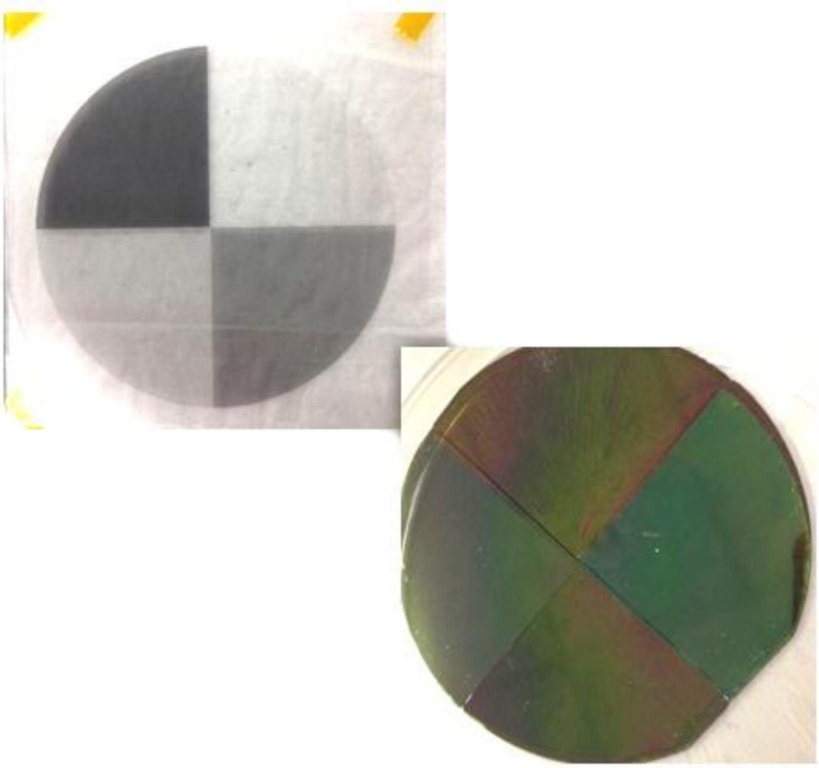

Figure 3.5 Patterned silicon wafer with PR on top and the corresponding mask

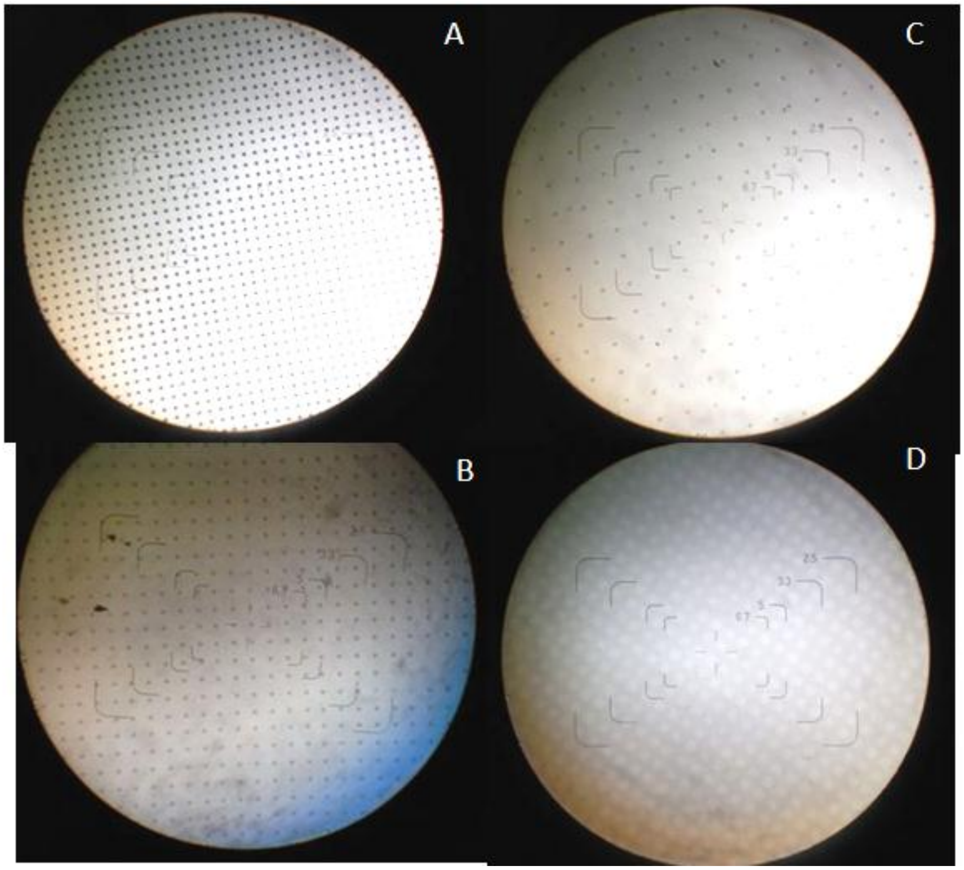

Figure 3.6 After PVD process before stripping off PR four different size of pattern under microscope using the same magnifying power

The optimized growth condition is set as the reaction temperature of the CVD chamber at 700 ℃, flow rate of C_2H_2:Ar at 20 sccm:75 sccm, and 20 min growth time after 5-min sputtering of Fe catalyst based on the earlier work [62]. To synthesize vertical aligned CNTs, 5-min sputtering of C after the layout of Fe catalyst is necessary. According to the SEM picture of the synthesis CNTs sample with different pattern size, it is verified that the pattern size is not affecting the construction of random CNTs. However even with 5-min C catalyst deposition, pattered wafer fails to grow vertical CNTs in the selective area. It all falls back to random CNTs category with no obvious difference between the batches with and without C catalyst deposition. For the purpose of showing an example, SEM pictures of CNTs sample in the 0.5 inch x 0.5 inch pattern square are shown in Figure 3.7.

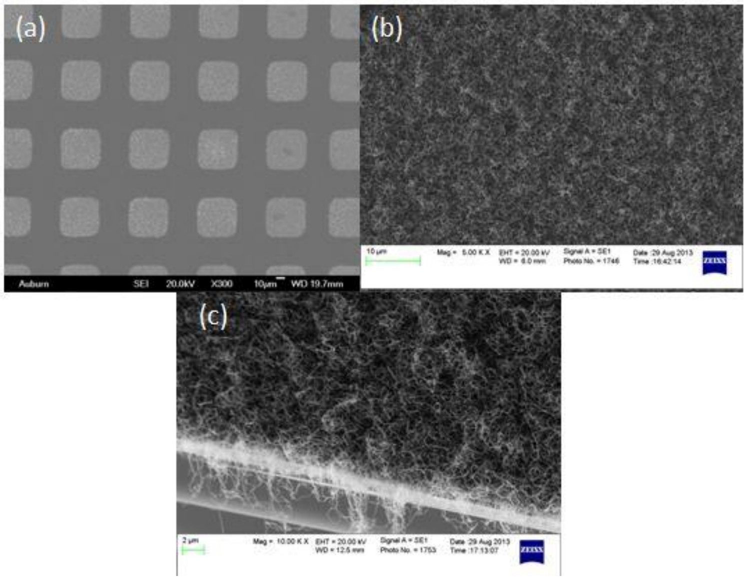

Figure 3.7 SEM pictures of patterned CNTs sample (a) x300 resolution to show the pattern layout on the wafer (b) x5000 resolution (c) cut-edge of CNTs sample in the patterned square

The field emission test is performed by another master student's work with the data curve shown in Figure 3.8 [84]. The turn-on voltage is smaller in pattern D with bigger pattern area and same saturation current density for all four cases. For the following device assembling, pattern D with 50 μm x50 μm square is selected in pursuit of lower turn-on voltage and maximum current emission capability.

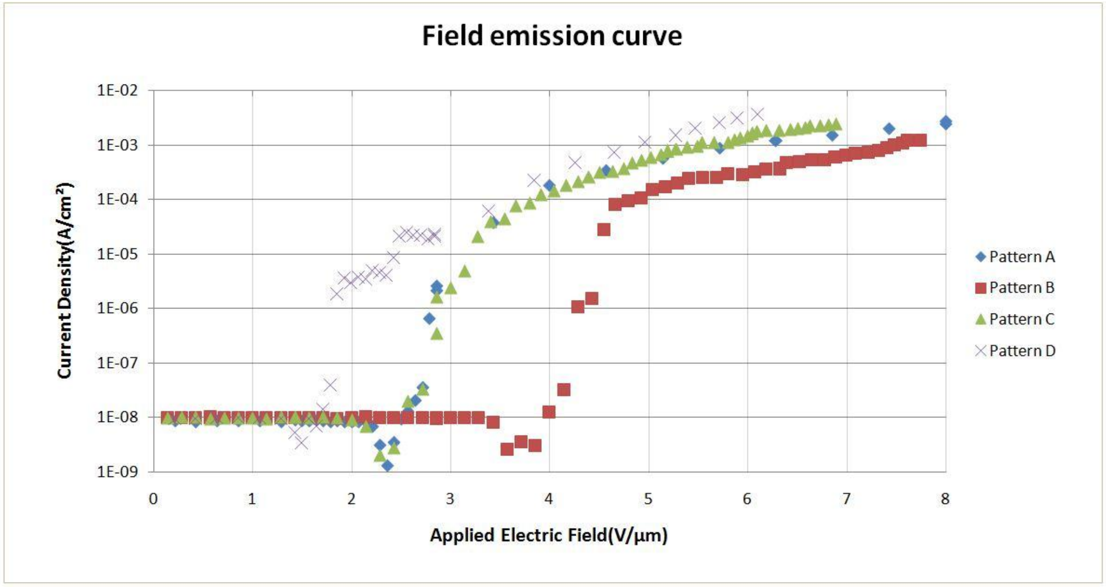

Figure 3.8 Field emission curves of four different patterned CNTs [92]

Chapter 4

Microplasma Device: Design, Construction and Testing

4.1 Chamber Construction and Diagnostic System Set-up

In this work four different types of microplasma devices were designed, constructed and tested. In all devices, the most common geometry is that they all contain cathode with drilled holes, cooper plate anode and a Teflon^{TM} plate as the separation. Each device was tested in air, helium and argon as the background gas in a vacuum chamber. The cross section view of one device is shown in Figure 4.1 with the critical dimensions. The hole diameter of the hollow cathode geometry is 0.15 cm, and the aluminum plate as cathode has the thickness of 0.15 cm. The testing circuit of the microplasma devices is shown in Figure 4.2. A 4.5-MΩ ballast resistor is connected in series with the device to limit the current density, preventing free electrons from damaging the CNTs samples on the back of the cathode. A high voltage DC power supply from Glassman High Voltage, *inc* is used to provide the DC voltage from 0 V to 1 kV in the experiments. The diagnostic system consists of high-speed camera, ammeter, high voltage probe, oscilloscope, and pressure gauge. The P5100 passive high voltage probes with 1000X attenuation factor is used to measure the plasma voltage. The M485 auto-ranging picoammeter from Keithley is inserted in the circuit to record the current flow. Four different constructions of the cathode with specific features are show in Figure 4.3.

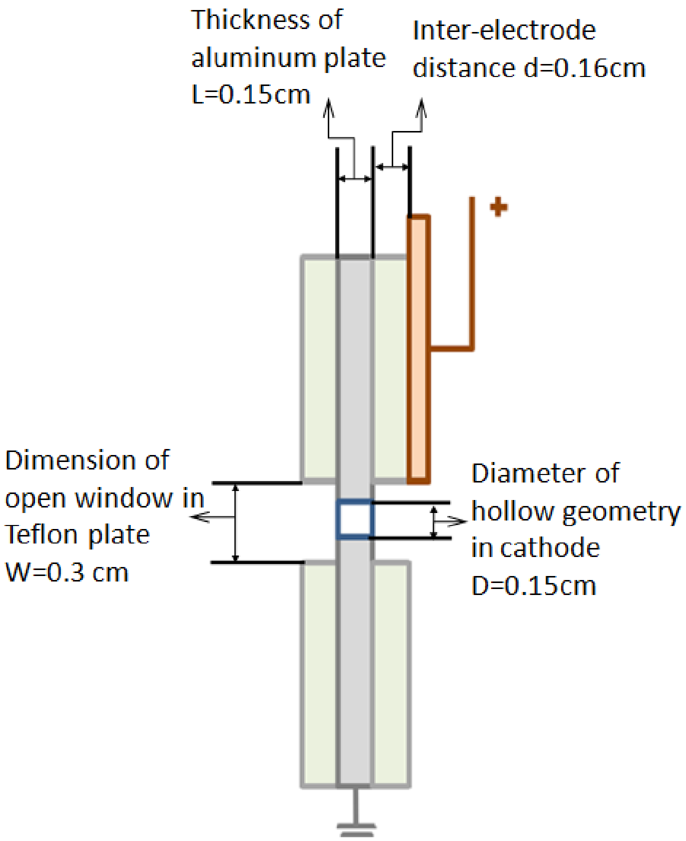

Figure 4.1 Microplasma devices' cross section with the critical dimensions

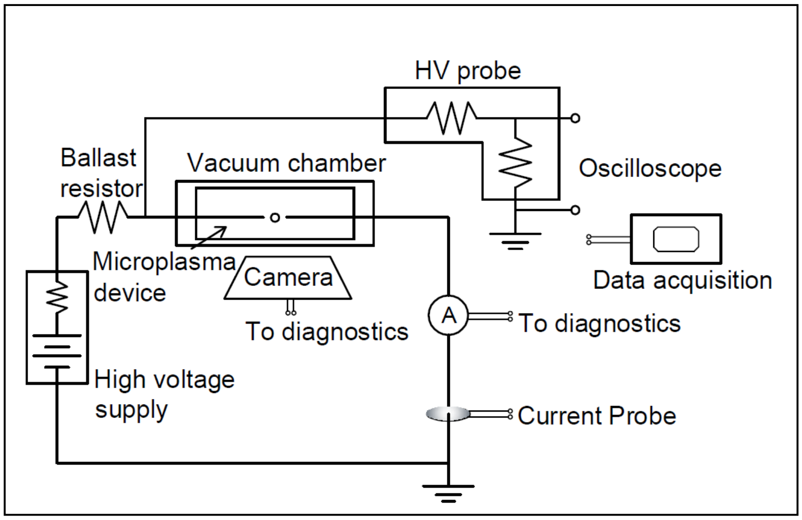

Figure 4.2 Microplasma devices' testing circuit

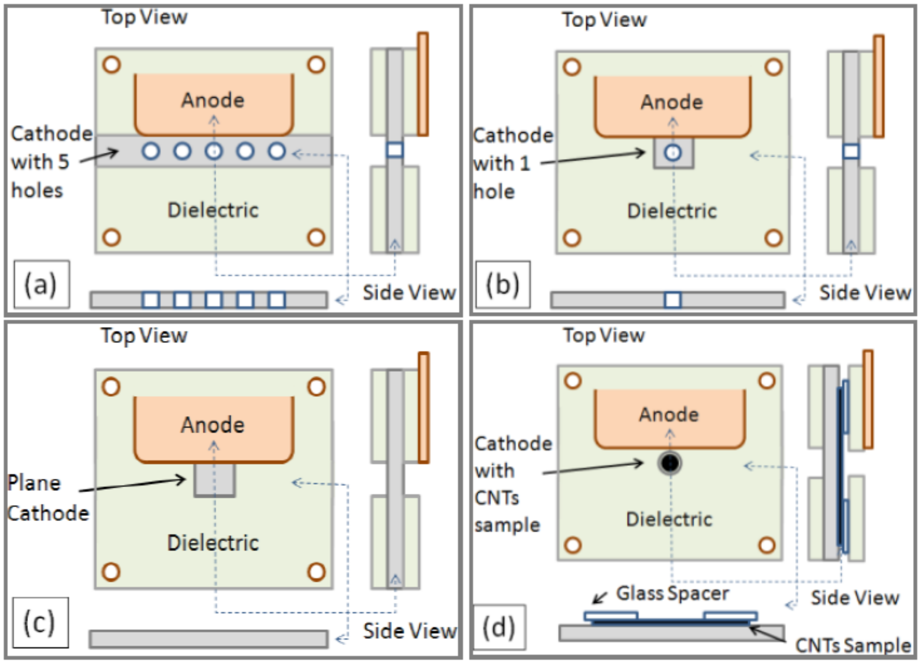

Figure 4.3 Different constructions of the cathode in microplasma devices (a) Hollow cathode with 5-hole, the distance between the adjacent hole is 0.5 cm ; (b) Hollow cathode with 1-hole; (c) Plane cathode with 1-hole; (d) CNTs integrated cathode geometry (all other dimensions are the same as shown in Figure 4.1)

4.2 Breakdown Voltage Test and Discussion

The breakdown voltages as a function of pressure are shown in Figure 4.4 for the different hollow cathode configuration (a) and (b) in air for the test purpose. The inter-electrode distance between the anode and the cathode remains the same in both cases shown as in Figure 4.1. For the cathode with 5 holes the breakdown voltage for the pressure range of 50 Torr~600 Torr is a straight line, which indicates that it is located on the right side of Paschen's curve. For the cathode with 1 hole, the breakdown voltage has both sides of Paschen's curve. Compared to the 1-hole cathode construction, the operating current is always higher for the 5-hole cathode one under the same applied voltage, which is caused by the larger discharge area. In the case of the microplasma produced by the 5-hole hollow cathode, not all the 5 holes are ignited at the same time by the applied voltage. The bright plasma formation is observed to shift from one hole to another without any specific change in the operating conditions. The voltage and current of the microplasma devices are also unstable with relatively large fluctuations. As the applied voltage increases, the frequency of the plasma moving in different locations is observed to increase too. Therefore, the 1-hole geometry is selected as the primary electrode configuration based on the stable operating conditions and lower operating current characteristics to protect the CNTs sample introduced later in the experiment.

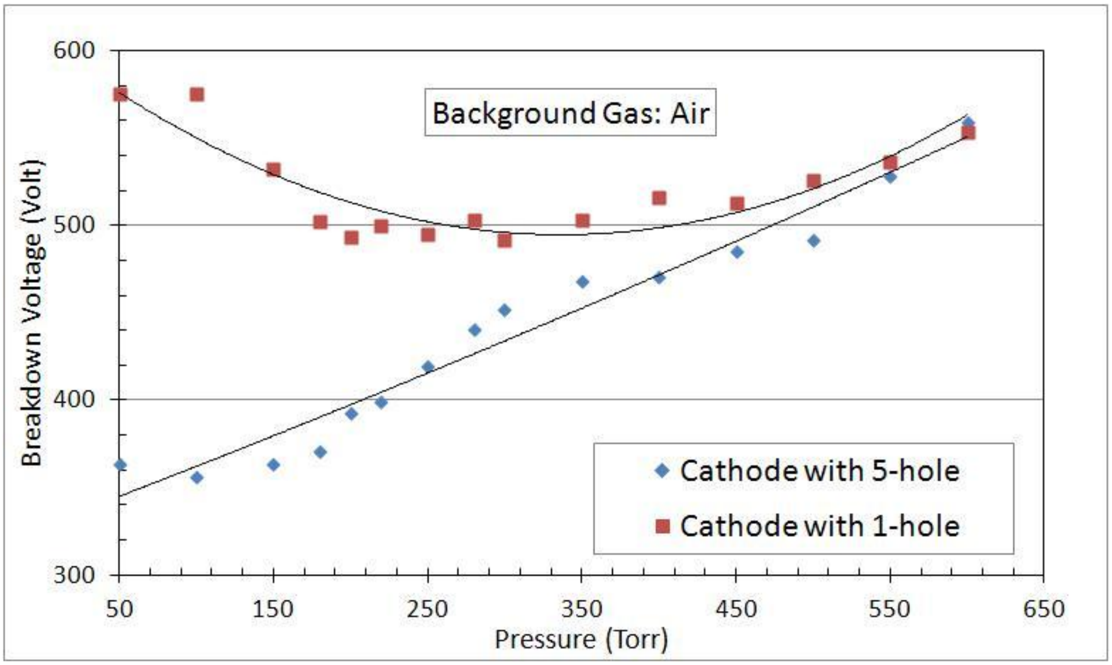

Figure 4.4 Breakdown voltage comparisons between hollow cathode with 1-hole and hollow cathode with 5-hole

The third geometry (c) is the plane cathode, where an aluminum plate is sandwiched between two Teflon^{TM} plates with one hole on each and operated as the plasma device in argon and helium. The comparison of the breakdown voltages for the hollow cathode with 1-hole and the plane cathode are shown in Figure 4.5. Both constructions follow similar characteristics in both gases. It is observed that the hollow cathode discharge has lower breakdown voltage compared to the plane cathode with a difference between 50 V and 250 V. This has been shown as the hollow cathode effect in the discharge process. Besides, the difference is more obvious in argon than that in helium. It indicates in helium, the ratio of electron mobility to atom mobility is smaller than that in argon. The virtual anode effect is not easily formed in hollow cathode geometry in helium. Argon is friendlier when working with hollow cathode discharge. The pressure when the breakdown voltage reached the minimum value for argon gas is around 200 Torr, while for helium it is around 400 Torr for both plane and hollow-cathode geometries. This indicates Paschen's law applies hollow cathode construction same as plane cathode one. Therefore, the voltage-current curves of these two cathodes are recorded in argon at 200 Torr pressure and in helium at 400 Torr (Figure 4.6), whose condition results in the minimum breakdown voltage to produce the plasma. Based on the record of the high-speed camera, argon plasma seems relatively more stable than helium one based on the higher mass of molecular and ion.

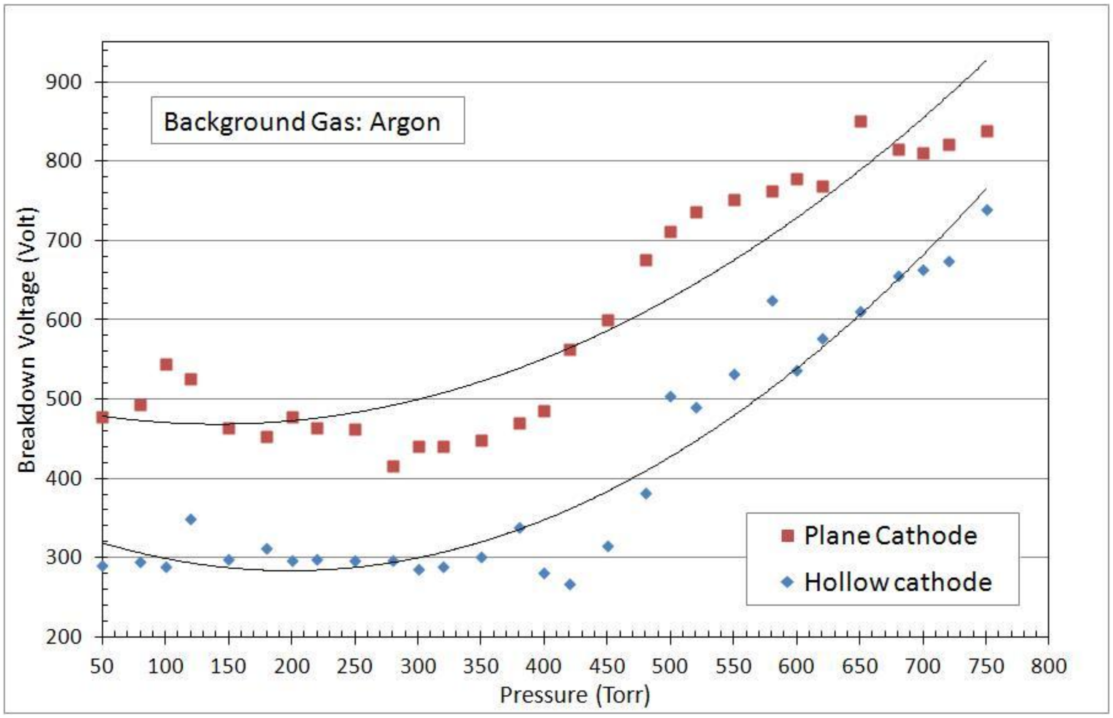

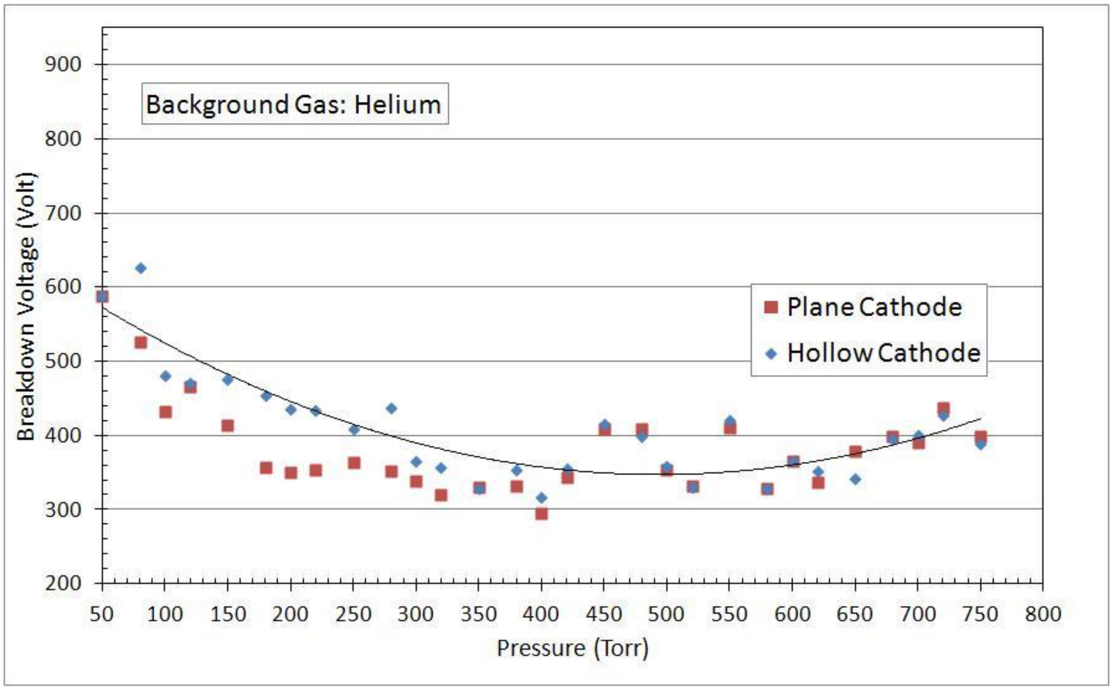

Figure 4.5 Breakdown voltage comparisons between hollow cathode and plane cathode with background gas of argon and helium.

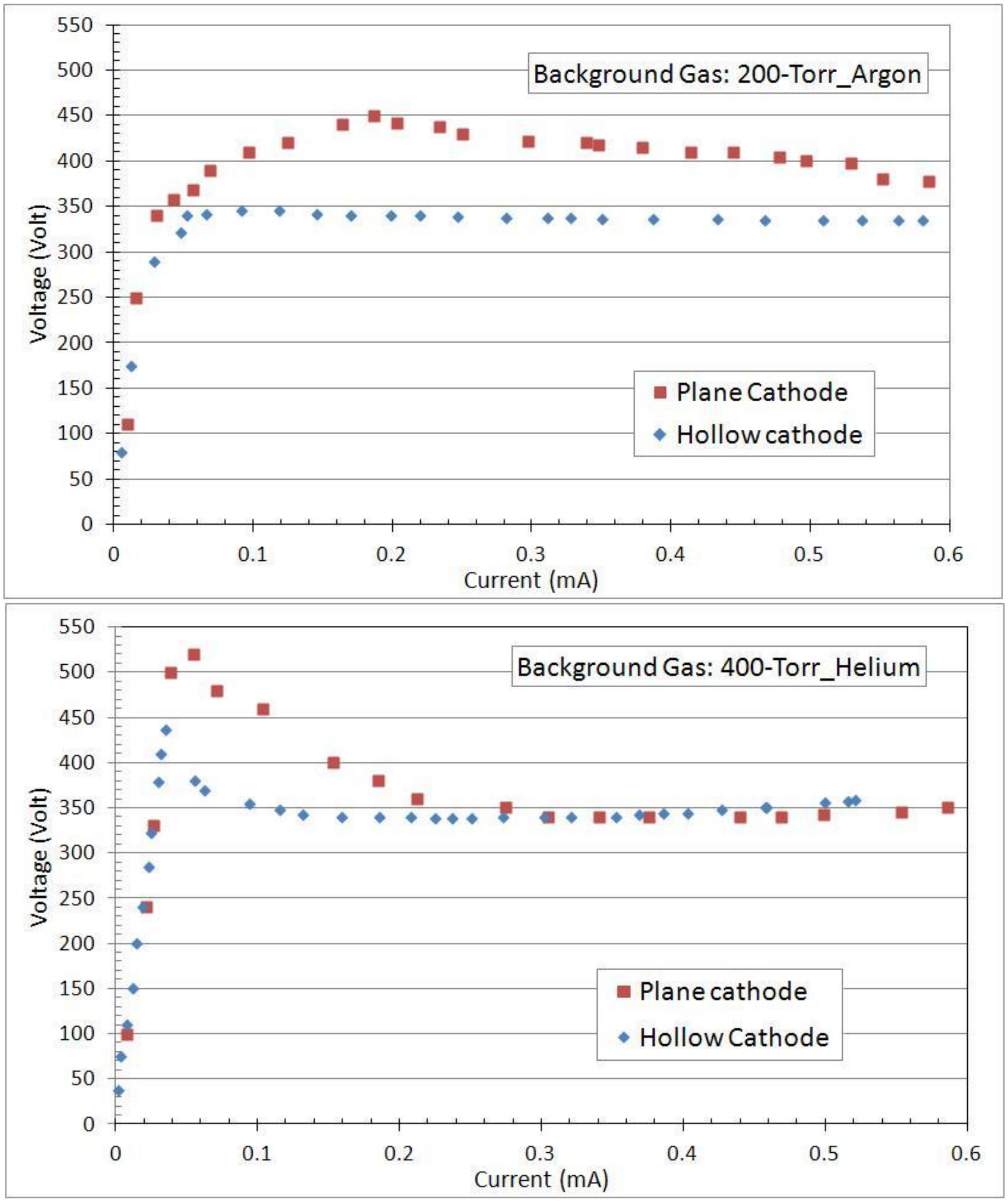

Figure 4.6 Voltage-current of the breakdown process under argon in 200 Torr pressure and under helium in 400 Torr pressure

Next the fabricated CNTs on Si wafer substrate is included in the design to study the electron emitter material's effect. The CNTs sample is synthesized under the sputtering condition of 5-min Fe and 20-min CVD growth with C_2H_2: Argon 25 sccm:75

sccm at 700℃. Unpatterned CNTs sample is adopted here since there is no concern for the integration of circuit at the first stage of development. The substrate containing the CNTs is placed on top of the aluminum plate and sandwiched between two Teflon^{TM} plates, with CNTs exposing to the electrical field through the hole on the Teflon^{TM} plate, shown as Figure 4.3 (d). The aluminum plate served as both the conducting surface to connect the CNTs with the power source and a heat sink for the CNTs. The voltage-current curves of the breakdown process are shown in Figure 4.7. The pictures taken by the high-speed camera are marked in the curves to show the pattern of the microplasma, corresponding to the voltage and current. The breakdown voltage in argon at 200 Torr is 380V, while that in helium at 400 Torr is 520 V. The breakdown voltage in argon is about 40 V smaller than that in hollow cathode without CNTs, while that in helium is the same as without. The discharge patterns didn't have any noticeable difference compared to that without CNTs based on the record by the camera. Hence, it is concluded that with the aid of CNTs the ignition voltage of the plasma can be reduced at least 10% in argon. However, not the same effect is observed in helium. In this case the current variation from 0.1 mA to 0.6 mA in both argon and helium is observed.

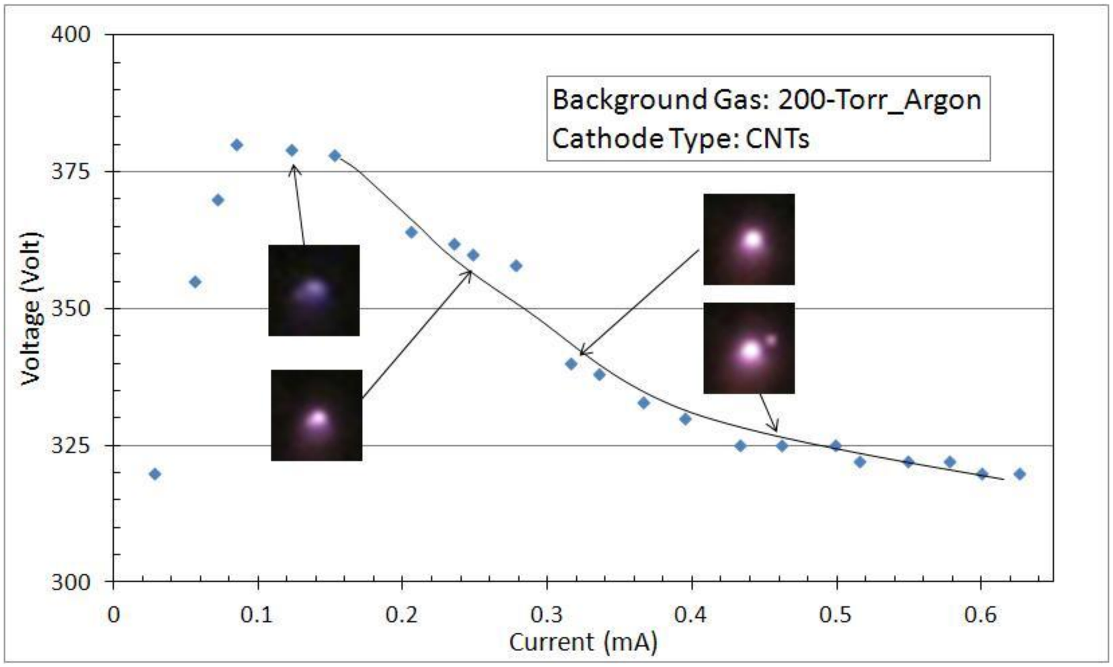

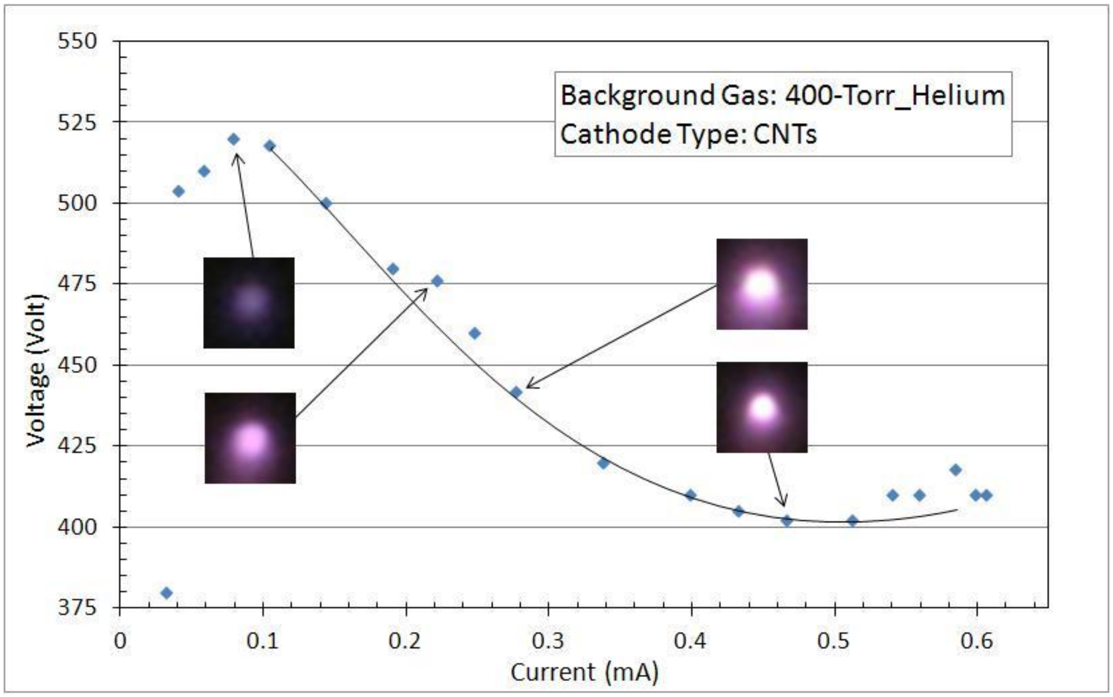

Figure 4.7 Voltage-current characteristics of the breakdown process with CNTs as the cathode under argon in 200 Torr pressure and under helium in 400 Torr pressure. The images are the corresponding plasma form at the given voltage and current conditions

Chapter 5

Pseudospark Switch

The pseudospark switch in this project consists of a U-shaped brass anode, a U-shaped copper cathode, both with a drilled hole in the center, and a CNT-coated trigger electrode attached to an aluminum plate. The switch design is shown in Figure 5.1 with the critical dimensions included. The anode is specially designed with the matching threads to the corresponding ceramic holder, therefore the distance between anode and cathode is adjustable and anode is stable in the set condition. The switch is enclosed in a double-ended MDC flange with a glass tube in the center so the plasma formation can be observed (Figure 5.2). Both a mechanical pump and a turbo pump are used to create the vacuum of 1×10^{-6} Torr as base pressure. A gas inlet is connected to the chamber through fine adjustment valve so the background gas, such as argon and helium, can be fed into the chamber. The operating pressure from a few mTorr to several Torr is achieved in the chamber. The trigger electrode has the easily demountable holder for different CNTs sample testing. An in-house constructed negative pulse generator is connected between the cathode and the trigger electrode, providing a negative pulse as high as 1 kV. Different level of negative pulse is produced by adjusting the charging current before producing the negative pulse, while different pulse width by changing the resistance in the discharging circuit. According to the tests, the pulse width of a single pulse is around 0.5 to 1 ms with the pulse voltage from 200 V to 1 kV (Figure 5.3). The HV350REG power supply is connected between anode and cathode, providing the high-regulated voltage from 0 V to 35 kV through an internal 22 MΩ current limiting resistor. The hollow cathode is connected to the ground while the chamber is isolated from all the electrodes components to keep the potential floating.

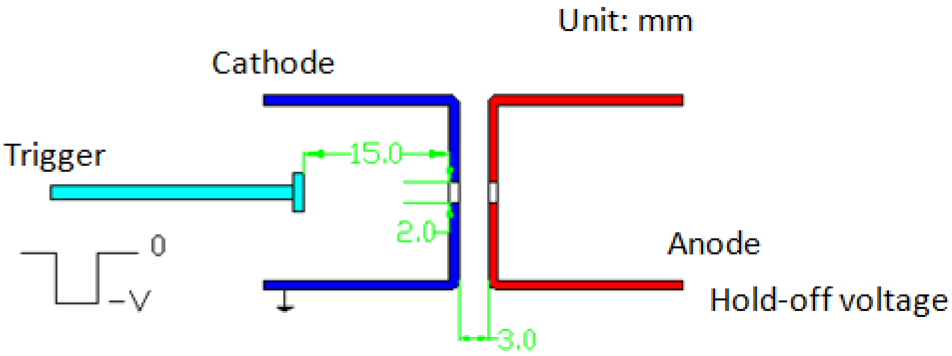

Figure 5.1 Sketch and critical dimensions of the constructed pseudospark switch

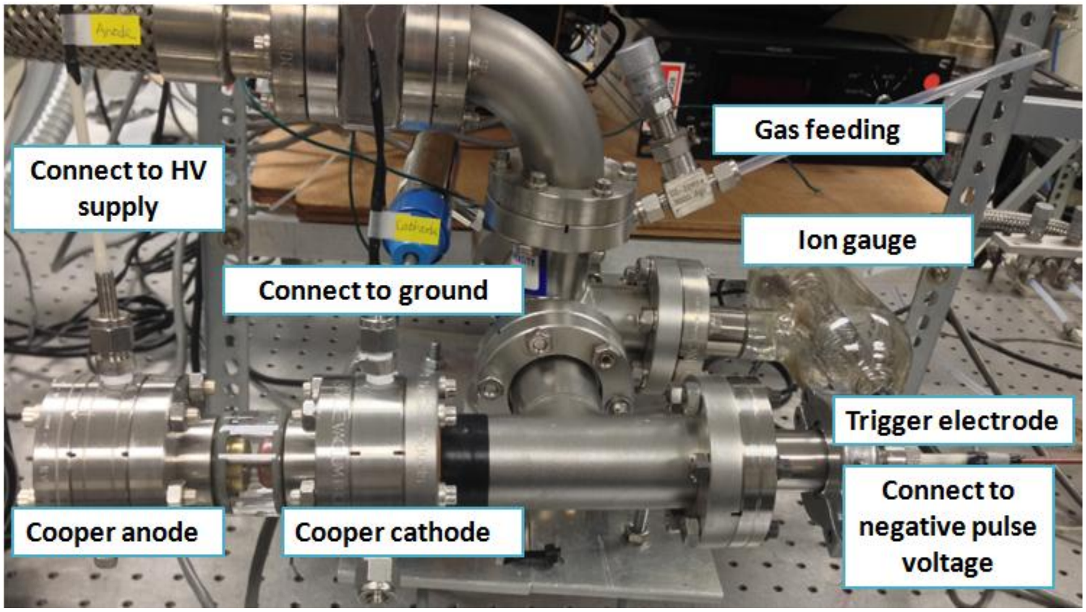

Figure 5.2 Assembled pseudospark switch chamber

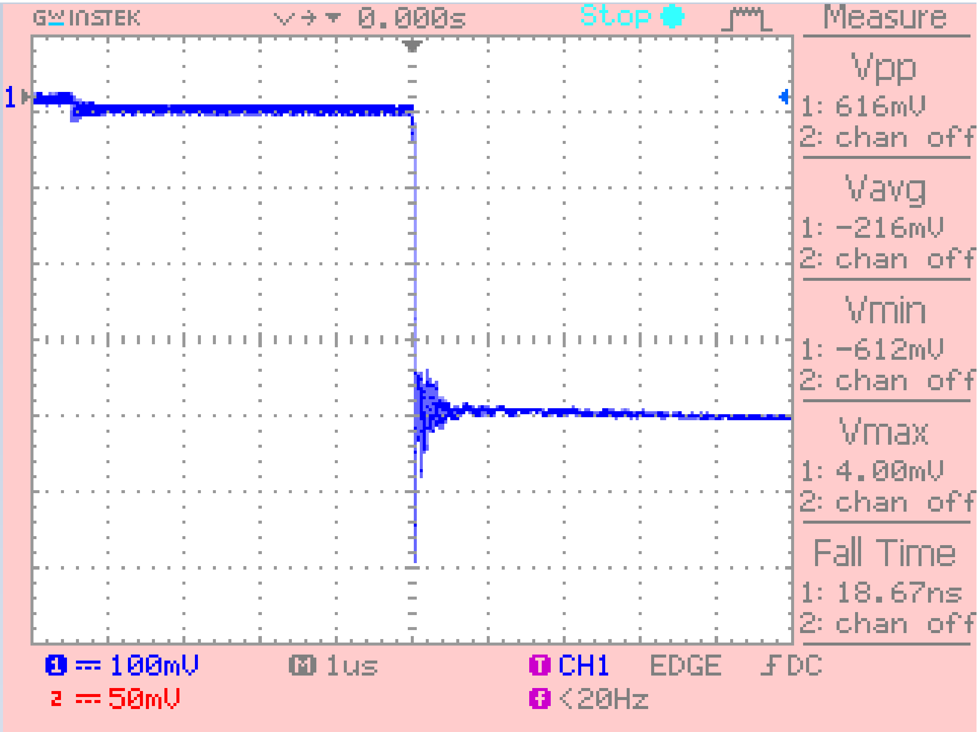

Figure 5.3 Applied negative pulse voltage

To characterize the performance of designed pseudospark switch, hold-off voltage, trigger delay time and jitter time are planned to be recorded based on different patterned CNTs' size. A high voltage attenuation probe Tektronix P6015 is used to record hold-off voltage, and B&K Precision PR2000 is used to record negative pulse voltage. A Rogowski current transformer is inserted in the circuit to measure the discharge current from anode to cathode. All the signals are captured through an oscilloscope for further analysis. The computer is connected to oscilloscope through a USB cable to collect the experimental data.

It is known that before the hold-off voltage testing process, the conditioning process needs to be performed in order to condition the high voltage electrode surfaces

[37]. This process reduces the impurities on the machined surfaces and helps to reduce the desorbed gases so the contamination in the chamber is reduced. The conditioning is performed by igniting the discharge at low current, which is normally referred as "plasma conditioning".

In order to present the influence of CNTs as electron emitter, we planned to firstly test constructed switch without the presence of CNTs triggering. Several initial tests have been conducted but no consistent data were captured. After examination, the high voltage DC power supply was found not functioning properly. It would short out and need to be reset each time. This behavior was the reason of inconsistency. The experimental studies were stopped at this point.

Our plans have been to test the switch with CNTs as the trigger electrode. For this we planned to use four different patterned CNTs samples, listed in Table 3.2 [84], and to analyze the effects of different pattern-size CNTs on hold-off voltage, trigger delay time and jitter time of the switch.

Chapter 6

Plasma Modeling using CNTs as Seed Electron Emitters

6.1 Plasma Processing Modeling

Applying CNTs as electron emitter material has recently become an active research field recently. In order to further understanding the mechanism and reactions in trigger processes and optimize the sources for applications, kinetic simulations are proposed to estimate the problem and meet the challenges. As a result of the tremendous improvements of the computer performance, development of computational plasma models has been done for nearly all types of plasmas, from low-pressure discharges for material surface treatment to atmospheric-pressure discharges for aeronautical flow control. Modeling has become increasingly important along with experimental diagnostics to characterize plasma in detail. Especially in microplasma, where the micro-level size geometry would confine the plasma, a detailed quantitative experimental diagnostics studies along with modeling is necessary. Therefore, many formulations have been brought out to model plasma processing discharges.

Normally three steps are crucial to perform a successful numerical analysis of any physical system [2]. The first step is to define the characteristic variables that best describe the physical problem. Secondly, the governing equations are selected to connect the variables based on different simulative models. Finally appropriate numerical method is brought up to solve the equation set, as well as the proper initial values and boundary conditions. Table 6.1 lists popular models and corresponding theoretic assumptions for plasma simulation. The fluid model is built based on assumption that energetic particles have gone through enough collision reactions to be characterized with a Maxwell-Boltzmann distribution. The kinetic model analyze the particle velocity distribution at every position by solving Maxwell-Boltzmann equation, but consumes more computational resources than fluid model. It is mostly used for plasma with low density of energetic particles [86]. To combine the advantages of both fluid model and kinetic model, hybrid model with Particle-In-Cell Monte-Carlo (PIC-MC) method is brought up to analyze plasma particles in different area [87].

Table 6.1 Different models and simulation methods for plasma

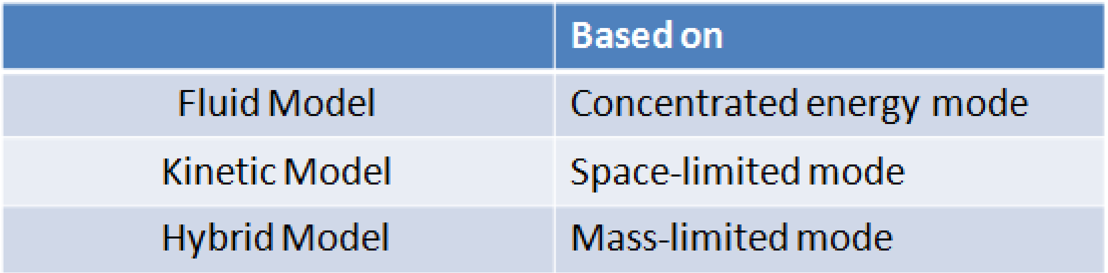

	Based on
Fluid Model	Concentrated energy mode
Kinetic Model	Space-limited mode
Hybrid Model	Mass-limited mode

To build a practical plasma model, a database of transport coefficients must be accessible with the accuracy. Assembling and maintaining the database and the proper reaction mechanisms are crucial to plasma modeling. The characteristics of a viable plasma model include easily defined geometries, material properties, and customized reaction chemistries. Besides, a correct surface kinetics modeling is necessary to make progress in modeling. Most rate coefficients are calculated either by experimental results of reaction cross-section area or by solving electron distribution function equation.

6.2 Fluid Model

Fluid model considers energetic particles in plasma as smoothed variables with mass and energy. It usually applies Navier-Stoke equations coupled with Poisson’s equation to solve electrons and ions partial differential equations. In this work the fluid model is adopted for modeling under subatmospheric pressure (10 mTorr) with the assumption that electron velocity/energy distribution function is close to Maxwell-Boltzmann distribution through high-frequency collisions. In this full continuum fluid model, the electrons' mean free paths are much smaller than the gradient length scales of the discharge properties. Therefore, it is reasonable to assume the discharge properties remain constant during the collision reaction. Since the simulation time is limited to several nanoseconds due to the available computational sources, the resonant excited species are ignored in this simulation; only long-lived electrons and ions are considered. The assumption includes that the contribution of the energy from the radiation of excited states is minor. The basic process of numerical techniques to simulate plasma is to cooperate the Poisson's equation of the electric field, the continuity equations of electrons, and the Navier-Stokes equations for the charged particles' dynamics. The shortcoming of this model is lack of ability to describe particles' movement in the presence of high electric field strength, such as cathode fall region in atmospheric-pressure plasma, where energetic particles are far from equilibrium with the electric field.

Table 6.2 10-mTorr argon plasma chemistry used in this work

Reactions	Reaction type	Energy loss [eV]	Reaction coefficient [m^3/s]
1. $Ar+e^{-1}=>Ar+e^{-1}$	Elastic collision	0	k_1
2. $Ar+e^{-1}=>Ar^{*}+e^{-1}$	Excitation	11.56	k_2 [88]
3. $Ar+e^{-1}=>Ar^{+1}+2e^{-1}$	Ionization	15.6	k_3 [89]
Electron generation rate R_e	$k_3 N_{n0} n_e$ [$1/(m^3 s)$]		
Energy lost rate S_e	$(11.56*k_2+15.6*k_3)N_{n0}n_e$ [$J/(m^3 s)$]		

The reaction coefficients are collected through National Institute for Fusion Science (NIFS) database (shown in Table 6.2 in detail). They are computed from cross-section data for each reaction with the assumption that electron energy level has a Maxwell-Boltzmann distribution under subatmospheric pressure.

$$k=\sqrt{\frac{2q}{m_e}}\int \varepsilon\sigma(\varepsilon)f(\varepsilon)d\varepsilon \tag{6.1}$$

where ε stands for electron energy (J), $f(\varepsilon)=\sqrt{\frac{m}{\pi kT_e}}e^{-\frac{\varepsilon}{kT_e}}$ is electron energy distribution function as Maxwell-Boltzmann distribution, $\sigma(\varepsilon)$ is the corresponding reaction cross-section (m^2), which is normally function of electron energy. Finally, the reaction coefficients are expressed in Arrhenius form as:

$$k = AT_e{}^B \exp\left(-\frac{C}{T_e}\right) \tag{6.2}$$

where A, B, and C are constants for corresponding reactions.

(1) Poisson's equation of the electric field

The electric potential is derived from Maxwell's equations and Poisson's equation.

Maxwell's extension of Ampere's law $\nabla\times\vec{H} = \sigma\vec{E} + \varepsilon\frac{\partial\vec{E}}{\partial t}$ (6.3)

where σ is conductivity of the material $\left(1/_{\Omega\cdot m}\right)$, ε is dielectric constant, or electrical permittivity $\left(F/_m\right)$. Let $\vec{H} = \frac{\vec{B}}{\mu} = \frac{\nabla\times\vec{A}}{\mu}$, where μ is magnetic permeability $\left(H/_m\right)$, $\vec{A}$ stands vector potential $\left(V\cdot s/_m\right)$. Substitute into equation (6.3)

$$\nabla\times\nabla\times\vec{A} = \mu\sigma\vec{E} + \mu\varepsilon\frac{\partial\vec{E}}{\partial t} \tag{6.4}$$

Substitute $\vec{E} = -\nabla\varphi - \frac{\partial\vec{A}}{\partial t}$

$$\nabla\times\nabla\times\vec{A} = \mu\sigma\left(-\nabla\varphi - \frac{\partial\vec{A}}{\partial t}\right) + \mu\varepsilon\frac{\partial}{\partial t}\left(-\nabla\varphi - \frac{\partial\vec{A}}{\partial t}\right) \tag{6.5}$$

Based on $\nabla\times\nabla\times\vec{A} = \nabla\left(\nabla\cdot\vec{A}\right) - \nabla^2\vec{A}$

$$\nabla\left(\nabla\cdot\vec{A}\right) - \nabla^2\vec{A} = \mu\sigma\left(-\nabla\varphi - \frac{\partial\vec{A}}{\partial t}\right) + \mu\varepsilon\frac{\partial}{\partial t}\left(-\nabla\varphi - \frac{\partial\vec{A}}{\partial t}\right) \tag{6.6}$$

According to Lorenz gauge condition, equation (6.6) is sought out by the following order.

$$\nabla\left(\nabla \cdot \vec{A}\right) = \mu\sigma\left(-\nabla\varphi\right) + \mu\varepsilon\frac{\partial}{\partial t}\left(-\nabla\varphi\right) \tag{6.7}$$

$$\nabla^2\vec{A} = \mu\sigma\frac{\partial\vec{A}}{\partial t} + \mu\varepsilon\frac{\partial^2\vec{A}}{\partial t^2} \tag{6.8}$$

Continue deriving equation (6.7).

$$\nabla\left(\nabla \cdot \vec{A} + \mu\sigma\varphi + \mu\varepsilon\frac{\partial\varphi}{\partial t}\right) = 0 \tag{6.9}$$

$$\nabla \cdot \vec{A} = -\mu\sigma\varphi - \mu\varepsilon\frac{\partial\varphi}{\partial t} \tag{6.10}$$

Based on Gauss's law, $\nabla \cdot \vec{E} = \frac{\rho}{\varepsilon}$, where $\rho = q\left(n_i - n_e\right)$ stands for charge density $\left({}^{C}\!/_{m^3} \right)$

$$\nabla\left(-\nabla\varphi - \frac{\partial\vec{A}}{\partial t}\right) = \frac{\rho}{\varepsilon} \tag{6.11}$$

$$\nabla^2\varphi + \frac{\partial\nabla \cdot \vec{A}}{\partial t} = -\frac{\rho}{\varepsilon} \tag{6.12}$$

Substitute equation (6.10) into equation (6.12)

$$\nabla^2\varphi - \mu\sigma\frac{\partial\varphi}{\partial t} - \mu\varepsilon\frac{\partial^2\varphi}{\partial t^2} = -\frac{\rho}{\varepsilon} \tag{6.13}$$

where $\sigma = n_e q\mu_e$, related to electron density and electron mobility.

(2) Continuity equations of electron

The electron density in plasma is determined by the electron continuity equation.

$$\frac{\partial n_e}{\partial t} + \nabla \cdot \left(-\mu_e n_e \vec{E} - D_e \nabla n_e \right) = R_e \tag{6.14}$$

where μ_e is the electron mobility $\left(m^2 / V \cdot s \right)$, D_e is the electron diffusion coefficient $\left(m^2 / s \right)$, and R_e is the electron generation rate through ionization reaction $\left(1 / m^3 \cdot s \right)$ as in Table 6.2. Normally the electron number flux is defined as the combination of drift and diffusion, $\vec{\Gamma_e} = -\mu_e n_e \vec{E} - D_e \nabla n_e$. Based on Einstein relation, electron diffusion coefficient and electron mobility have the relationship as follows:

$$D_e = \frac{\mu_e k_B T_e}{q} \tag{6.15}$$

Electron mobility is set to constant as 3 $m^2 / V \cdot s$ based on the density of background gas [68], which is determined by the ideal-gas law.

$$N_{n0} = \frac{P}{k_B T} \tag{6.16}$$

(3) Navier-Stokes equations for the gas dynamics

Navier-Stokes equation is derived from Newton's second law with conservation of momentum in mass and energy. The general form of Navier-Strokes in fluid motion is

$$\rho \left(\frac{\partial \vec{v}}{\partial t} + \vec{v} \cdot \nabla \cdot \vec{v} \right) = -\nabla p + \nabla \cdot \vec{T} + f \tag{6.17}$$

where $\vec{v}$ is the flow velocity, ρ is the fluid density, p is the pressure, $\vec{T}$ is the component of the total stress tensor, and f is body forces per unit volume acting on the fluid. This is applied to determine electron temperature. In order to coordinate the form of electron energy equation with electron continuity equation, several variables are introduced to simplify the equation.

Define electron energy density as n_l ("l" stands for level of energy) $\left({}^{J}\!/\!{}_{m^3} \right)$.

$$n_l = \frac{1}{2} m_e v^2 \cdot n_e = \frac{3}{2} k_B T_e n_e \tag{6.18}$$

$$\nabla n_l = \frac{3}{2} k_B \nabla (T_e n_e) = \frac{3}{2} k_B (T_e \nabla n_e + n_e \nabla T_e) \tag{6.19}$$

For electron energy flux in monatomic species as argon,

$$\overrightarrow{Q_l} = \frac{5}{2} k_B T_e \overrightarrow{\Gamma_e} - \frac{5}{2} k_B D_e n_e \nabla T_e \tag{6.20}$$

where the first term is the electron energy flux from the electron flux, and the second term stands for the heat flux from gradient of electron temperature with the thermal conductivity in electron flux as $\lambda_e = \frac{5}{2} k_B D_e n_e$. To connect the electron energy flux with the electron energy density, define μ_{el} is the electron energy mobility $\left({}^{m^2}\!/\!{}_{V \cdot s} \right)$, D_{el} is the electron energy diffusion coefficient $\left({}^{m^2}\!/\!{}_{s} \right)$.

$$\mu_{el} = \frac{5}{3} \mu_e \tag{6.21}$$

$$D_{el} = \frac{5}{3} D_e \tag{6.21}$$

$$\begin{aligned} \overrightarrow{Q_l} &= \frac{5}{2} k_B T_e \overrightarrow{\Gamma_e} - \frac{5}{2} k_B D_e n_e \nabla T_e = \frac{5}{2} k_B T_e \left(-\mu_e n_e \vec{E} - D_e \nabla n_e \right) - \frac{5}{2} k_B D_e n_e \nabla T_e \\ &= -\frac{5}{2} k_B T_e \mu_e n_e \vec{E} - -\frac{5}{2} k_B D_e (T_e \nabla n_e + n_e \nabla T_e) = -\mu_{el} n_l \vec{E} - D_{el} \nabla n_l \end{aligned}$$

$$\overrightarrow{Q_l} = -\mu_{el} n_l \vec{E} - D_{el} \nabla n_l \tag{6.23}$$

The corresponding electron energy equation is

$$\frac{\partial n_l}{\partial t} + \nabla \cdot \overrightarrow{Q_l} + q \overrightarrow{\Gamma_e} \cdot \vec{E} = S_e \tag{6.24}$$

where $q\overrightarrow{\Gamma_e} \cdot \vec{E}$ stands for Joule heating of electron in electrical field, S_e is energy lost rate in inelastic collisions between electrons and neutrals (ionization and excitation) $\left(J \middle/ m^3 \cdot s \right)$ as in Table 6.2.

To solve the above equations set, the initial values of the variables and proper boundary conditions need to be defined. There is no direct supportive experimental data to verify electrons in subatmospheric plasma having a Maxwell distribution. It has been observed a deviation from a Maxwell electron energy distribution in lower pressure microplasma with a high-energy tail [90]. At higher pressure, the distribution is known to be less deviated due to shorted Debye length [91]. Therefore it is still justified assumption to simulate subatmospheric-pressure plasma behavior under a Maxwell electron energy distribution. To express the effect of CNTs as emitter material, the plasma vanishing process is chosen for the sake of simplicity of model. The initial electron density is set as $10^{15}\ 1/m^3$ with Maxwell distribution. The initial electron temperature is set as $1\ eV$. The Debye length of this model is $\lambda_D = \sqrt{\frac{kT_e\varepsilon_0}{n_e e^2}} = 0.235mm$.

Because of the sheath effect, the density of electrons is usually considered as a small constant at the boundaries with consistent electron energy. The secondary electron emission effect is omitted here since the free electron influx from CNTs is the priority to consider. Therefore, the boundary condition for electron density is limited as follows:

$$\overrightarrow{\Gamma_e} \cdot \vec{n} = \frac{1}{4} v_{e,th} n_e \tag{6.25}$$

where $\vec{n}$ represents the normal direction of the boundary, pointing towards the wall, $v_{e,th} = \sqrt{\frac{8k_B T_e}{\pi m_e}}$ represents the mean speed of electron movements in Maxwell distribution. In order to save the time and sources of simulation, at boundary between electrodes and argon gas T_e is set as 300 K in the model. The ions' movement is considered as heavy particles' flux, limited by the mobility conditions. Therefore, the boundary condition for ion density is limited as follows:

$$\overrightarrow{\Gamma_i} \cdot \vec{n} = \mu_i n_i \vec{E} \cdot \vec{n} \tag{6.26}$$

At the trigger cathode, where CNTs sample sits in, the influx of free electrons is added to exhibit the effects of CNTs as electron emitter in the experimental setup. The influx is expressed as:

$$\overrightarrow{\Gamma_e} \cdot \vec{n} = \frac{I}{q \cdot S_{CNTs}} \tag{6.27}$$

where I stands for the emission current from CNTs sample under certain amount of trigger voltage [84], S_{CNTs} stands for the effective area of CNTs sample $\left(m^2\right)$.

The applied voltage defines electrical field's boundary condition. Dirichlet boundary condition is a fixed boundary condition. It is adopted for electrical potential distribution to specify the values of applied voltage along the boundary of trigger, cathode and anode. The finite element analysis is adopted here to calculate the equation set to solve electrical field distribution, electron density and electron temperature. The experimental geometry is in axisymmetric cylindrical form. A non-uniform grid is built in order to make sure plenty of resolution is present near boundaries to signify the high gradient in plasma sheath (Figure 6.1). The 2mm-diameter pseudo-anode is built at the opposite side of cathode to simulate the effect of actual U-shaped anode in the experimental set-up.

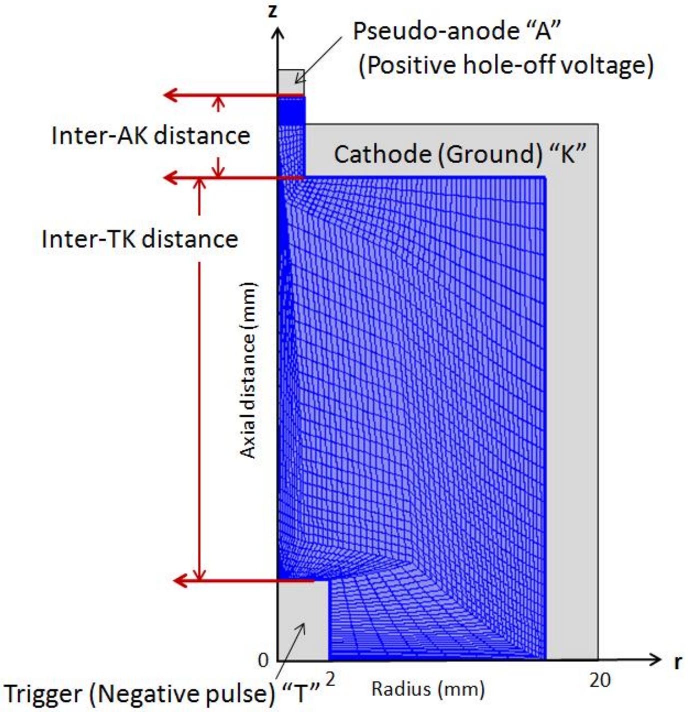

Figure 6.1 Schematic diagram of the computational domain with meshes

6.3 Results and Discussion

In order to investigate the optimized operating conditions in the pseudospark switch, different distances between trigger and cathode electrode and the distance between anode and cathode electrode (shown as "Inter-TK distance" and "Inter-AK distance" respectively in Figure 6.1) are executed in simulation. Simulation is performed under 10mTorr pressure, 100V negative pulse voltage triggering and 500 V positive hold-off voltage for three different cases (shown in Table 6.3). The CNTs influx is estimated by the field emission test of CNTs sample applied in the experiments based on triggering voltage's level.

Table 6.3 Three cases for 10-mTorr argon plasma discharge development with listing parameters.

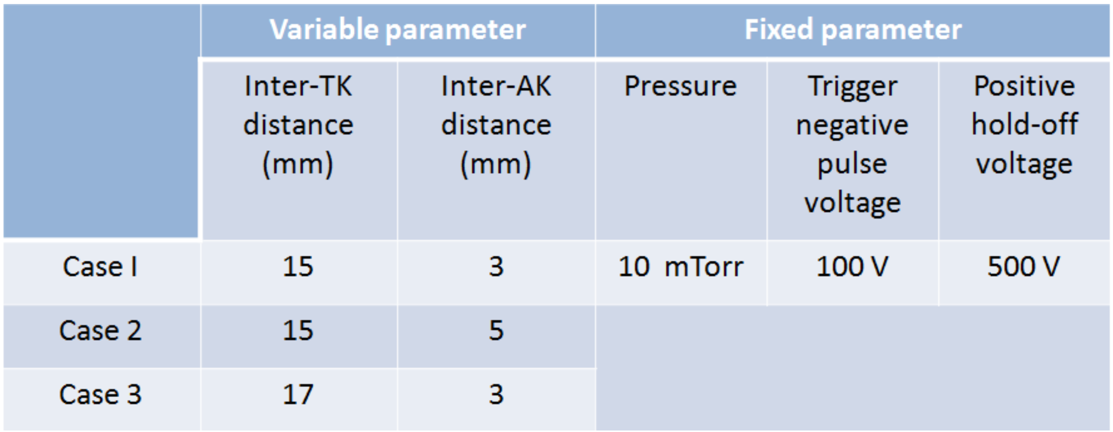

	Variable parameter		Fixed parameter		
	Inter-TK distance (mm)	Inter-AK distance (mm)	Pressure	Trigger negative pulse voltage	Positive hold-off voltage
Case I	15	3	10 mTorr	100 V	500 V
Case 2	15	5			
Case 3	17	3			

Figure 6.2 shows along symmetric z-axis (r=0) voltage distribution at time t=0, 0.0001 ns, 0.001 ns, and 0.01 ns respectively in three cases successively, while Figure 6.3 shows electrical field distribution z-component. Generally speaking, the discharge could be considered as two continuous glow discharges respectively from trigger to cathode and from cathode to anode. The voltage profile shows a consistent drop of ~100 V at the trigger side and ~500 V drop at the cathode side, which are corresponding to cathode dark space in glow discharge. The negative glow region is identified as almost flat potential distribution, where electron density is matched by ion density with an equal order of magnitude by excitation mainly. By comparison between Case 1 and Case 3,

the inter-TK distance doesn’t affect the voltage distribution profile with the same cathode sheath in both trigger and cathode sides, which is approximately three times the Debye length of the plasma. The larger inter-AK distance in Case 2 gives the rise of potential distribution above 500 V with lower electrical field z-component. In glow discharge, the electrical field strength must be sufficient to produce energetic electrons for ionization process to replace those electrons that diffuse to the walls. With same anode applied voltage in Case 1 and Case 2, the electrical field strength is lower in Case 2 because of bigger inter-AK distance. As the anode is approached, adjustment such as random electron current may be forced to be larger to suit anode current. Since ion density in this model is considered as constant in the volumetric plasma because of much lower mobility than electrons, a positive ion sheath may be formed caused by drawing extra electron current from the plasma to anode. That may cause the raised voltage in the vicinity of anode electrode. The results indicate that the formation of increasing voltage near anode is depending on the details of specific discharge. The more realistic model should include ion density variable in the simulation to observe the voltage distribution by Poisson's equation. In Figure 6.3, the electrical field strength shows the peak at the anode surface for all three cases. The Faraday dark space appears as electrons become relatively slow and unable to react and begin to feel the existence of positive anode potential. It is identified with the slight decrease in the electrical field strength at 1 mm distance from the trigger surface and at 1 mm distance from the anode surface no matter what inter-TK and inter-AK distances are.

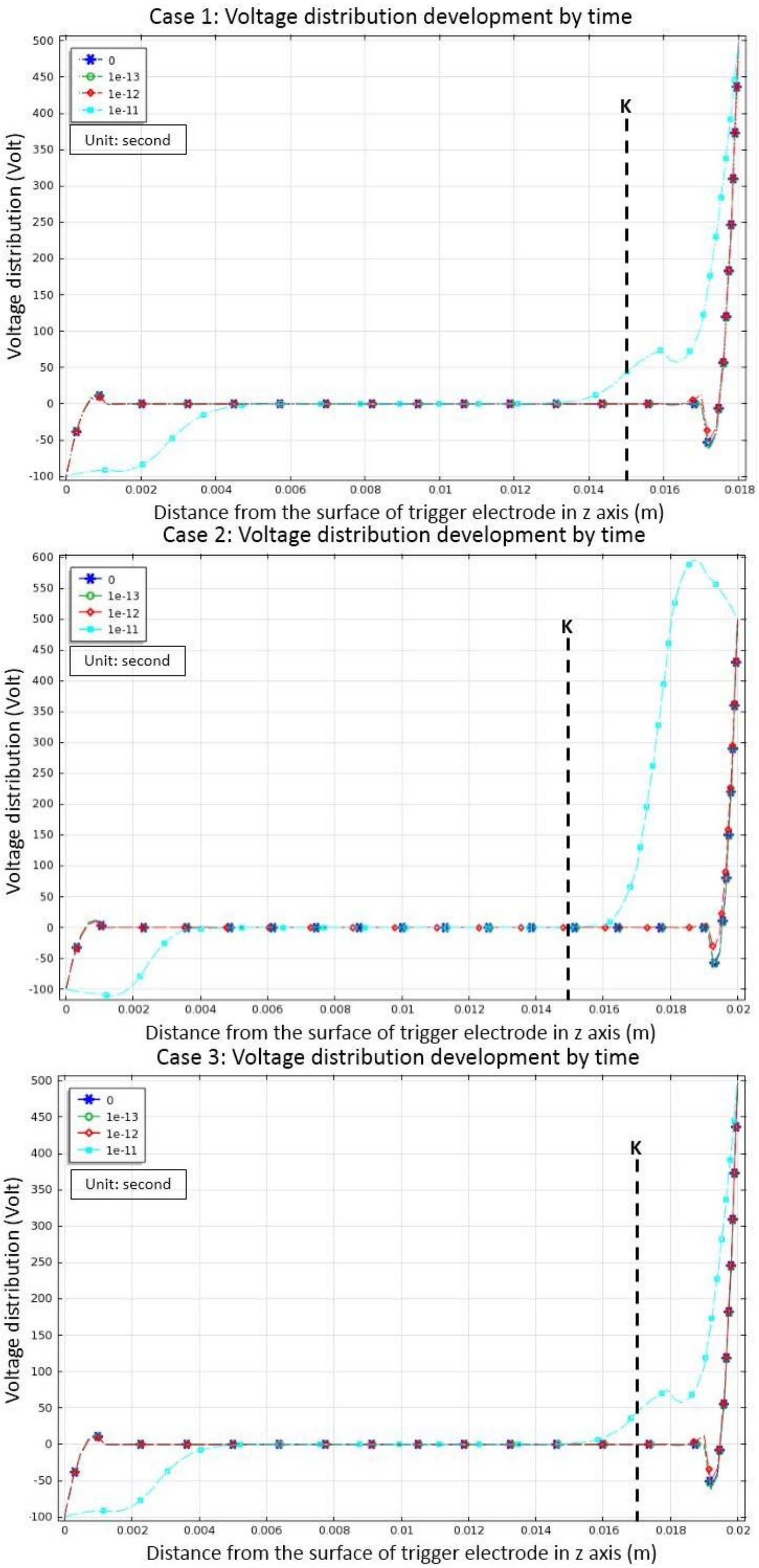
Case 1: Voltage distribution development by time

Case 2: Voltage distribution development by time

Case 3: Voltage distribution development by time

Figure 6.2 Plot of voltage distribution history along the symmetry axis from the surface of trigger to the surface of pseudo-anode for three cases

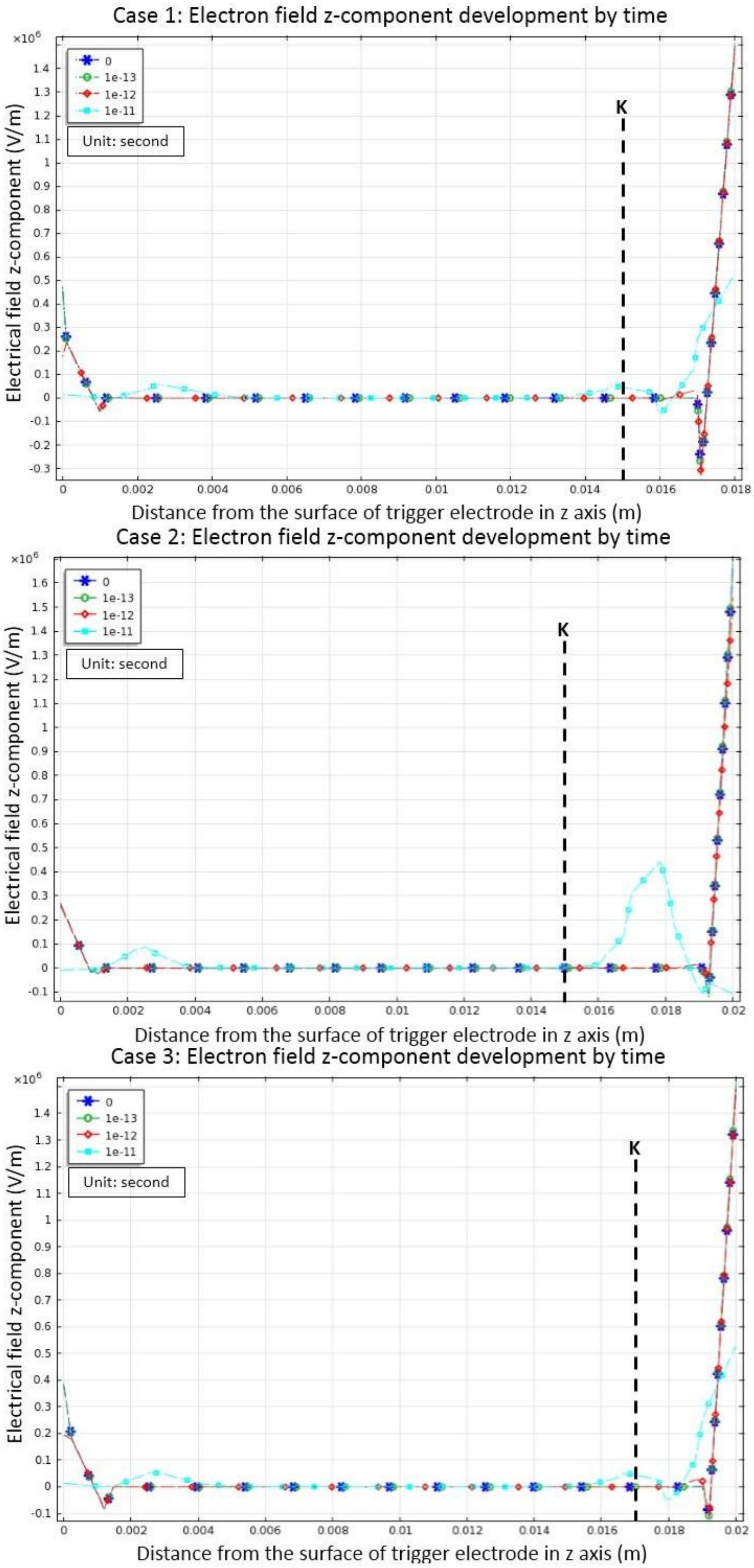

Figure 6.3 Plot of electrical field z-component history along the symmetry axis from the surface of trigger to the surface of pseudo-anode for three cases

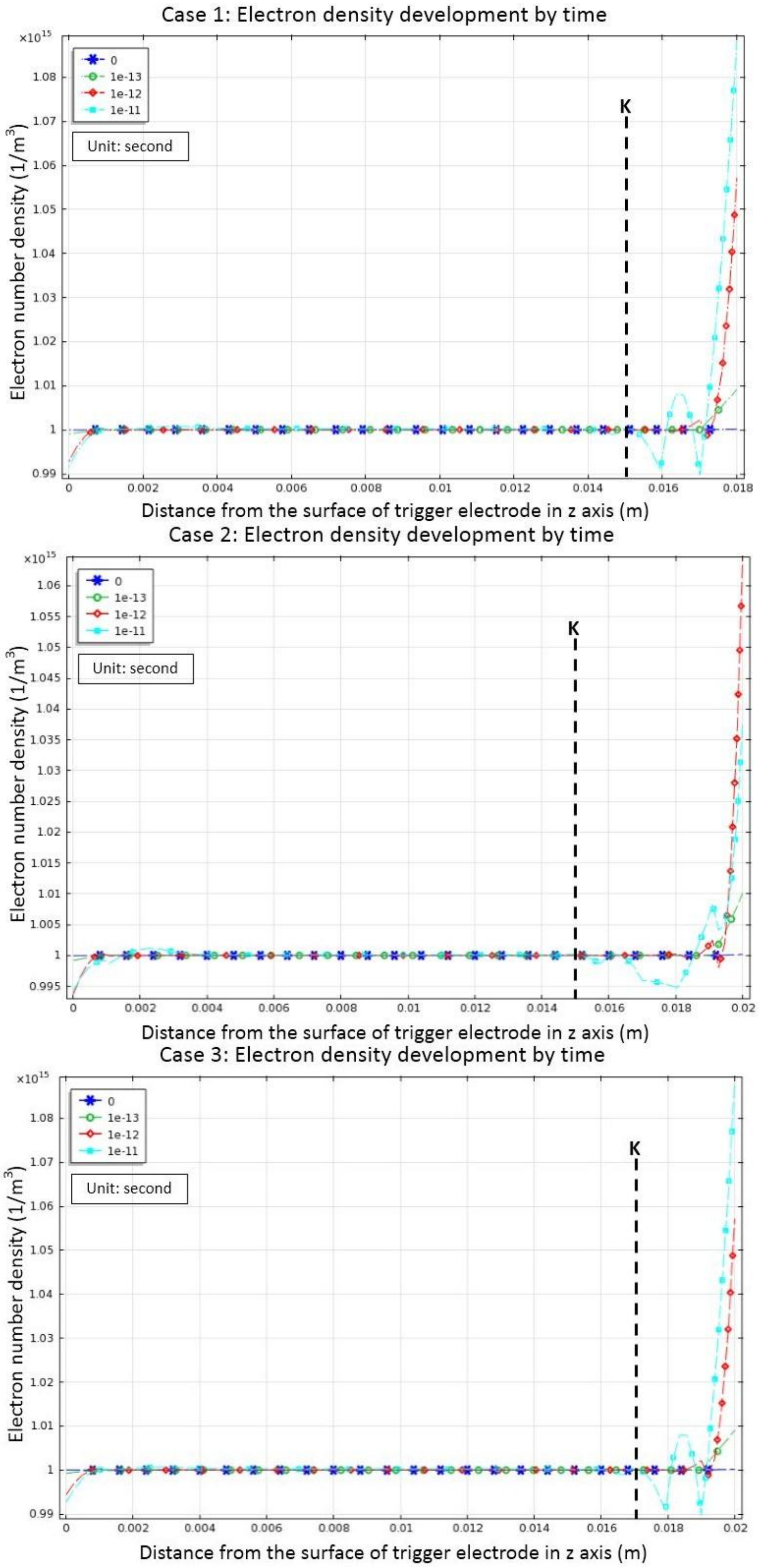

Figure 6.4 Plot of electron density history along the symmetry axis from the surface of trigger to the surface of pseudo-anode for three cases

Figure 6.4 shows electron density development in the same consistent order as voltage distribution and electrical field z-component. Three points are picked in the construction of the chamber (Figure 6.5) to investigate the electron density development by time (Figure 6.6). As Figure 6.4 indicated, the profile shows peak electron density at anode surface at any case, instead of around cathode glow area next to cathode surface in normal glow discharge. It is caused by the influx added in the trigger side in this work to simulate the role of CNTs in the experiment. In fluid model, the plasma volume is considered as fluid with the continuous flow by Navier-Stroke equation. Because of the extra electron source added in the trigger side, the accumulation of electrons is built up at the other side of the plasma volume, behaving like the fluid in a pipe. With limited reaction coefficient adopted in this simulation work, the volumetric production of electrons is conquered by the extra source added on the trigger surface, which coincidences the purpose of this simulation to characterize the effects of CNTs as electron emitter in the plasma production. The profile of electron density basically fits to the tendency of electron field z-component distribution in any case. This is because of the energy gained by electron is mainly from applied voltage. As Figure 6.6 Case 1 and Case 3 shown, even with longer propagation path for electrons flow from trigger to cathode, there is no divergence in electron number density's development by selected position. In all three cases, the electron number density stays constant level in the vicinity of cathode surface due to effect of grounded cathode. In the vicinity of anode surface, electron number density keeps growing tendency in Case 1 and Case 3, while that starts dropping after 0.0015 ns in Case 2. To achieve the purpose of switch-on and lower jitter-time in the switch design, higher electron number density at the anode side is demanded by confining the distance between anode and cathode. As Case 1 and Case 3 indicated, the inter-TK distance doesn't affect electron number density distribution. As the inter-AK distance grows, the absorption of electron density in the vicinity of anode is more obvious in Case 2 compared to that in Case 1. Figure 6.7 shows the electron temperature development in the same consistent order as electron density. The same distribution profile fits Case 1 and Case 3. As the inter-AK distance grows in Case 2, the pseudo-anode performs the function of heat-sink with lower electron temperature on the anode side.

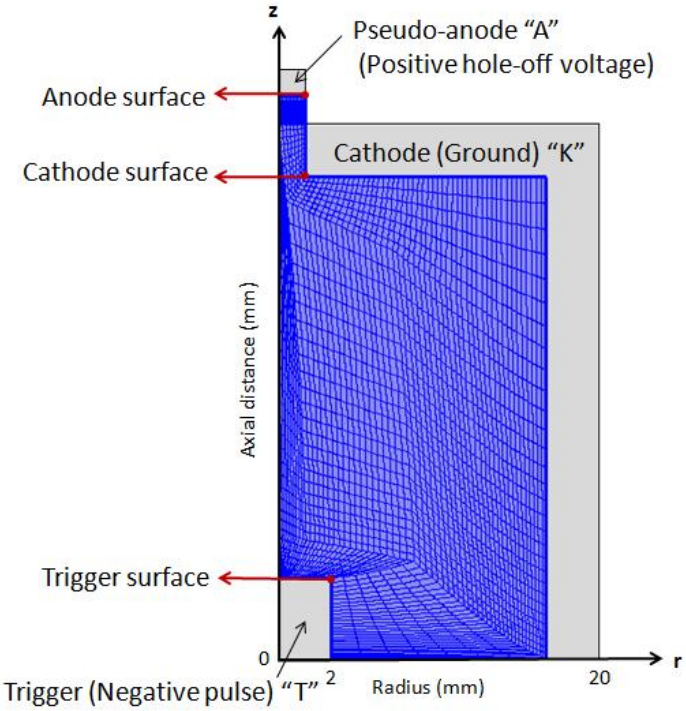

Figure 6.5 Three points in the construction of chamber to investigate the electron density development by time

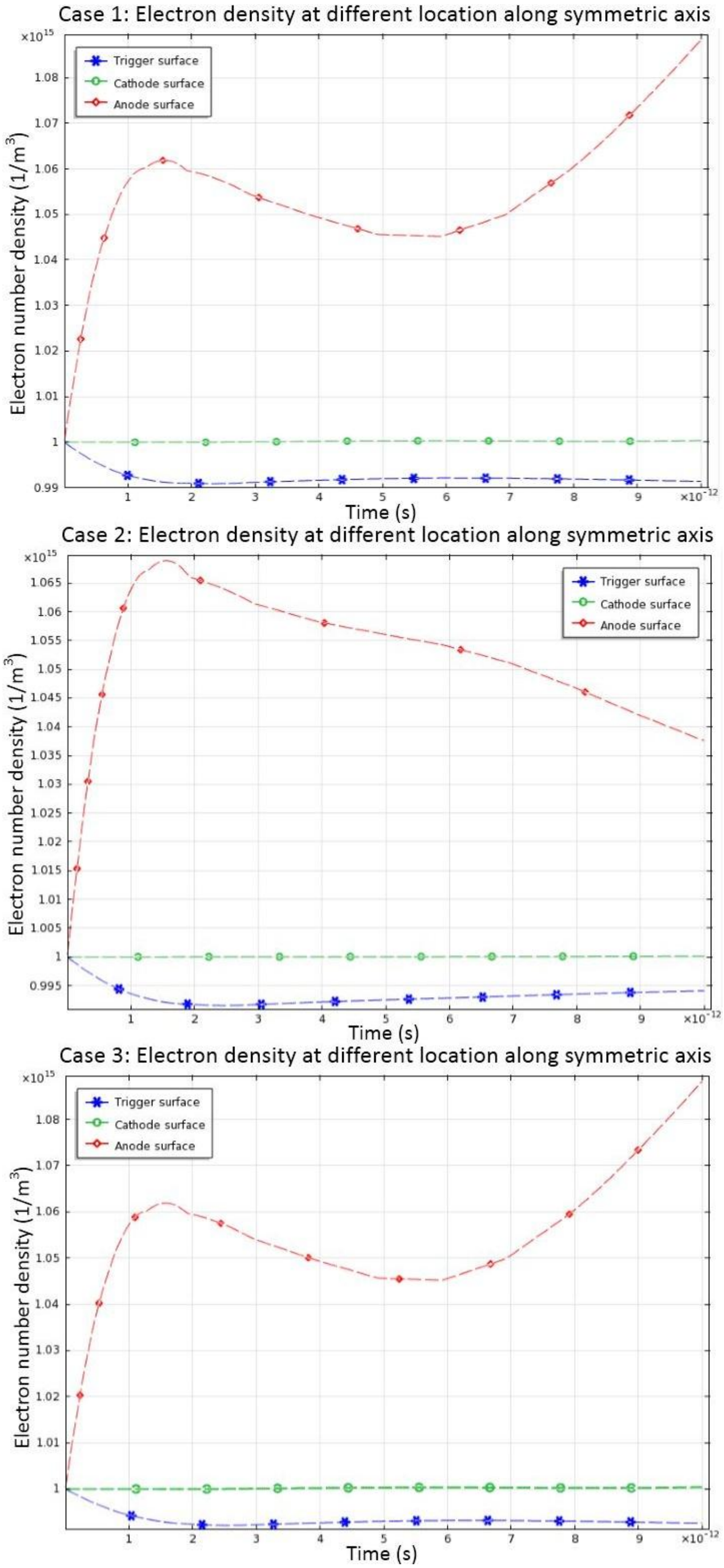

Figure 6.6 Plot of electron density development by time for three cases

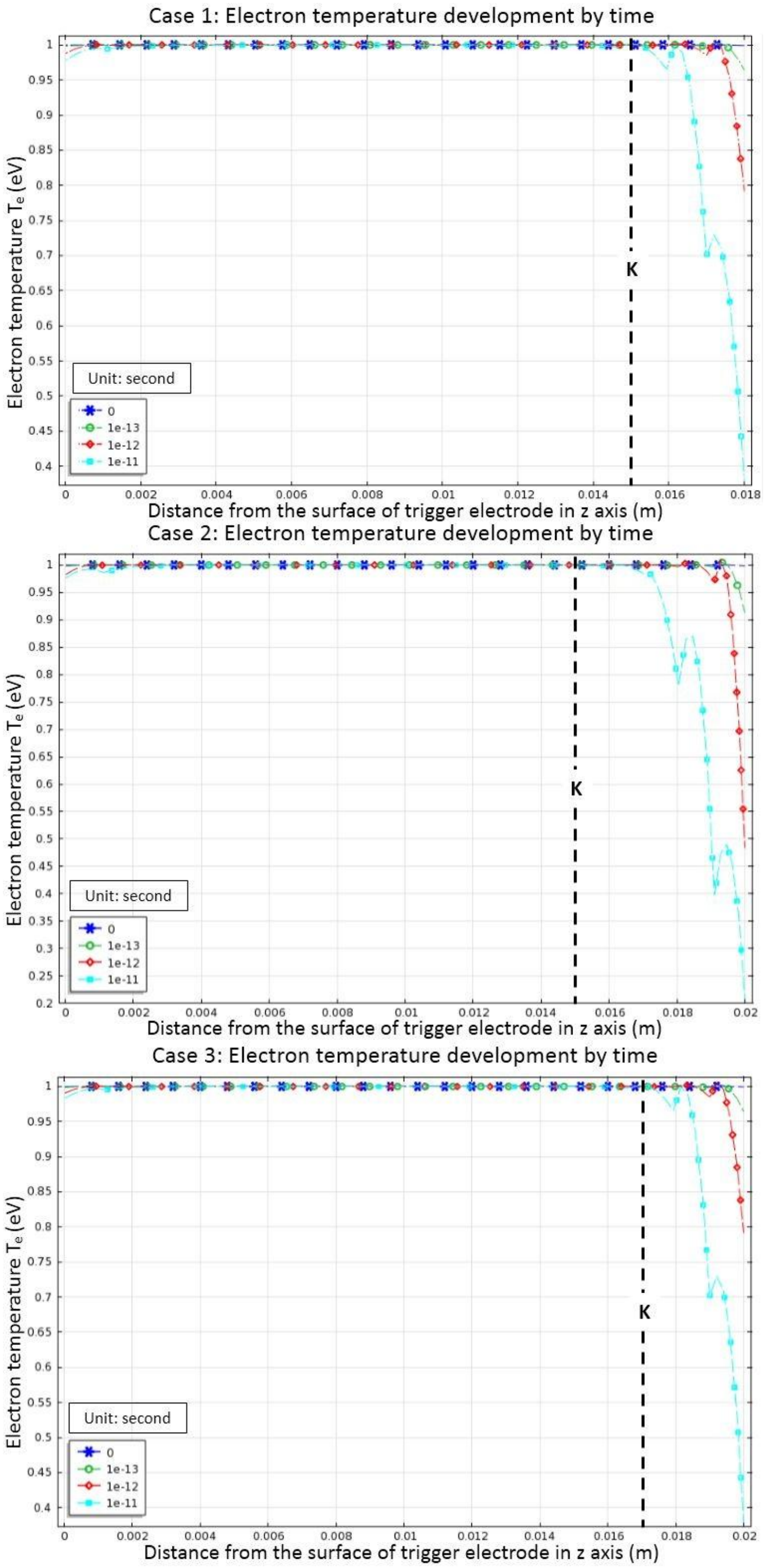

Figure 6.7 Plot of electron temperature history along the symmetry axis from the surface of trigger to the surface of pseudo-anode for three cases

In spite of the simple fluid theory adopted in this model, simulated numerical results shows consistence with tube glow discharge pattern. The simulation shows a stable glow discharge sustained by the influx added on the trigger electrode. Electron number density reaches peak concentration at the anode side to assist the switch process in the 1 ps time and with high electron number density. The results indicate that it is beneficial for the operation of the switch with limited inter-distance between hollow cathode and anode. The position of trigger electrode inside the hollow cathode construction doesn't affect neither the profile of electron number density nor the electrical field distribution.

Because of limited computational resources and time frame, the work is focused on the plasma dying out process, with starting point of electron number density equal to 10^{15} $1/m^3$. The future work should be developed to investigate the initiation of the plasma with the aid of CNTs placed at the trigger electrode. Besides, more accurate assumption should be introduced into the simulation, such as adding one more variable of ion density in the model. As pressure goes up to more than subatmospheric level, kinetic model and hybrid model should be introduced to investigate the behavior of the energetic particles with varying mobility and diffusivity in the one-free-path distance.

Chapter 7

Summary

Subatmospheric pressure plasma has caught more and more research interests due to the advantages of easier construction and stable operation. Two different subatmospheric plasmas devices, microplasma with hollow cathode structure and pseudospark switch, are designed and studied in this research. To optimize the performance of plasma devices, it is necessary to raise the number of emitter electrons to ignite the discharge process. CNTs as a cold electron emitter material are applied in both microplasma devices and pseudospark switch to achieve optimized working conditions.

Four cathode constructions are built and tested in the study of microplasma devices, which include a hollow cathode with 5 holes, a hollow cathode with 1 hole, a plane cathode, and CNTs-integrated cathode constructions. Based on the results, all four cathode-geometries succeeded in producing microplasma in both argon and helium. The cathode with CNTs is verified to have lower breakdown voltage than others in argon. Compared to the hollow cathode geometry, the breakdown voltage of the plane cathode is relatively higher at constant pressure. Also we observed differences in the operating characteristics of the same cathode in helium or argon as the background gas. The minimum breakdown voltage of the hollow cathode in argon is found to be lower than that in helium. This is a promising preliminary finding showing that CNTs can be applied as electron emitter for microplasma devices.

Pseudospark switch is designed and constructed with CNTs as trigger source, hollow cathode and hollow anode for application in the pulsed power system. Square patterned CNTs samples are applied on the surface of trigger electrode as cold electron emitter source. A two dimensional fluid model is built and solved based on the finite element analysis method. The characteristics of the free electrons emitted from CNTs samples are investigated in the cathode cavity by simulation. The Maxwell-Boltzmann electron energy distribution function is adopted to express the initial condition of free electrons in the chamber. The decay process of the plasma in the cavity is simulated and presented under applied electrical field and the free electrons influx from CNTs sample. The results indicate that the two consistent discharge patterns are occurring from trigger to cathode and from cathode to anode respectively as glow discharge in a tube. Based on the distribution of electron number density, the cathode dark space and negative glow region are identified in the vicinity of both trigger electrode and cathode. Under the same operating conditions, the inter-distance between trigger and cathode doesn't affect the distribution of electron number density and electric field, while to confine the distance between cathode and anode is beneficial to stabilize the plasma in the switch.

Reference

[1] J Reece Roth, "Industrial Plasma Engineering Volume 1: Principles", *Institute of Physics Publishing Bristol and Philadelphia*, 1995.

[2] A. P. Papadakis, S. Rossides and A. C. Metaxas, "Microplasmas: A review", *The Open Applied Physics Journal*, vol. 4, pp. 45-63, 2011.

[3] Sabnavis Bindu Madhav, "Microplasma MEMS device: Its design, fabrication and application in hydrogen generation for fuel cells", *Master Thesis*, Center for material science and engineering, Rochester Institute of Technology, Rochester, New York, August 12, 2009.

[4] Ramesh Bokka and Hulya Kirkici, "Field emission degradation of carbon nano-tubes", *in the Proceedings of 2010 IEEE International Power Modulator and High Voltage Conference*, pp. 594-597, 2010.

[5] G Mechtersheimer, R Kohler, T Lasser and R Meyer, "High repetition rate, fast current rise, pseudo-spark switch", *Journal of Physics E: Scientific Instruments*, vol. 19, No. 6, pp. 466-470, 1985.

[6] W. Platte, "Pulse shaping by laser-excited solid-state plasma in silicon", *Electronics Letters*, vol. 12, No. 23, pp. 631-633, November 1976.

[7] V. I. Molotkov, A. P. Nefedov, M. Yu. Pustyl'nik, V. M. Torchinsky, V. E. Fortov, A. G. Khrapak, and K. Yoshino, "Liquid plasma crystal: coulomb crystallization of cylindrical macroscopic grains in a gas-discharge plasma", *JETP Letters*, vol. 71, No. 3, pp. 102-105, 2000.

[8] S. Fujioka, H. Nishimura, H. Takabe, N. Yamamoto, K. Nishihara, D. Salzmann, T. Norimatsu, N. Miyanaga, K. Mima, H. Azechi, A. Sunahara, Y. Shimada, Y. Izawa, K. Nagai, F. Wang, J. Zhong, G. Zhao, Y. Li, Q. Dong, S. Wang, Y. Zhang, J. Zhang, Y-J Rhee, Y-W Lee, D-H. Kwon, "Laser-produced plasmas as unique X-ray sources for industry and astrophysics", *Journal of Physics: Conference Series 244*, 2010.

[9] E. Barborini, P. Piseri, and P. Milani, "A pulsed microplasma source of high intensity supersonic carbon cluster beams", *Journal of Physics D: Applied Physics 32.21*, L105-L109, 1999.

[10] E. E. Kunhardt, "Generation of large-volume, atmospheric-pressure, nonequilibrium plasmas", *IEEE Transactions on Plasma Science*, vol. 28, No. 1, pp. 189-200, February, 2000.

[11] Davide Mariotti and R Mohan Sankaran, "Microplasma for nanomaterials synthesis", *Journal of Physics D: Applied Physics*, vol. 43, pp.1-21, 2010.

[12] A. D. White, "New hollow cathode glow discharge", *Journal of Applied Physics*, vol. 30, No. 5, pp. 711-719, May. 1959.

[13] Karl H Schoenbach, Ahmed El-Habachi, Wenhui Shi, and Marco Ciocca, "High-pressure hollow cathode discharges", *Plasma Sources Sci. Technol. 6*, pp. 468-477, June 1997.

[14] V. V. Zhurin, "Hollow cathodes: Part 1", *Vacuum Technology & Coating*, pp. 28-35, September 2012.

[15] D. J. Sturges and H. J. Oskam, "Studies of the properties of the hollow cathode glow discharge in helium and neon", *Journal of Applied Physics*, vol. 35, No. 10, pp 2887-2894, October 1964.

[16] Alexander Fridman and Lawrence A. Kennedy, "Plasma Physics and Engineering", Second edition, *CRC Group*, Taylor & Francis Group, 2010.

[17] P. F. Little and A. von Engel, "The hollow-cathode effect and the theory of glow discharges", *in the Proceedings of the Royal Society of London Series A, Mathematical and Physical Sciences*, pp. 209-227, June 1954.

[18] G Stockhausen and M Kock, "Proof and analysis of the pendulum motion of beam electrons in a hollow cathode discharge", *Journal of Physics D: Applied Physics*, vol. 34, pp. 1683-1689, 2001.

[19] Prashanth S. Kothnur and Laxminarayan L. Raja, "Two-dimensional simulation of a direct-current microhollow cathode discharge", *Journal of Applied Physics 97*, 043305, 2005.

[20] Qiuping Zhou, Cheng Cheng, and Yuedong Meng, "Electron density and temperature measurement by Stark Broadening in a cold argon arc-plasma jet at atmospheric pressure", *Plasma Science and Technology*, vol. 11, No. 5, October 2009.

[21] D. Mariotti and K. Ostrikov, "Tailoring microplasma nanofabrication: from nanostructures to nanoarchitectures", *Journal of Physics D: Applied Physics*, April 2009.

[22] Ling-Guo Meng, Hai-Feng Liang, Chun-Liang Liu and Zhi-Hu Liang, "A line array of microplasma devices with coplanar electrodes operating in argon", *IEEE Transactions on Plasma Science*, vol. 36, No. 5, pp. 2788-2794, Octorber 2008.

[23] Karl H. Schoenbach, Ahmed El-Habachi, Mohamed M. Moselhy, Wenhui Shi and Robert H. Stark, "Microhollow cathode, discharge excimer lamps", *Physics of Plasm*a, vol. 7, No. 5, pp. 2186-2191, May 2000.

[24] J. G. Eden, S-J Park, N. P. Ostrom and K-F Chen, "Recent advances in microcavity plasma devices and arrays: a versatile photonic platform", *Journal of Physics D: Applied Physics*, pp. 1644-1648, May 2005.

[25] S-J. Park, J. Chen, C. Liu, and J. G. Eden, "Silicon microdischarge devices having inverted pyramidal cathodes: Fabrication and performance of arrays", *Applied Physics Letters*, vol. 4, No. 78, pp.419-421, Jan. 2001.

[26] C. G. Wilson and Y. B. Gianchandani, "Led-SpEC: Spectroscopic detection of water contaminants using glow discharge from liquid electrodes", *IEEE Trans. Electron Devices*, vol. 49, No. 12, pp. 2317-2322, Dec. 2002.

[27] K. Shimizu, T. Sugiyama, M. Nishamani and M. Kanamori, "Application of microplasma for NO_x removal", *IEEE Transactions on Industry Applications*, vol. 45, No. 4, pp. 1506-1512, July/August 2009.

[28] C. G. Wilson and Y. B. Gianchandani, "Selective deposition of silicon at room temperature using DC microplasma", *IEEE Transactions on Plasma Science*, vol. 35, No. 3, pp. 573-577, June 2007.

[29] M. Blajan, A. Umeda, S. Muramatsu and K. Shimizu, "Emission spectroscopy of pulsed powered microplasma for surface treatment of PEN film", *IEEE Transactions on Industry Applications*, vol. 47, No. 3, pp. 1100-1107, May/June 2011.

[30] Ahmed El-Habachi and Karl H. Schoenbach, "Generation of intense excimer radiation from high-pressure hollow cathode discharges", *Applied Physics Letters*, vol. 73, No. 7, pp 885-887, August 1998.

[31] M. S. Naidu, and V. Kamaraju, "High voltage engineering, 2nd edition", *McGraw Hill*, 1995.

[32] Davide Mariotti, Yoshiki Shimizu, Takeshi Sasaki, and Naoto Koshizaki, "Gas temperature and electron temperature measurements by emission spectroscopy for an atmospheric microplasma", *Journal of Applied Physics*, vol. 101, 013307, January 2007.

[33] M. P. Gomes, B. N. Sismanoglu, and J. Amorim, "Characterization of microhollow cathode discharges", *Brazilian Journal of physics*, vol. 39, No. 1, pp. 25-30, March 2009.

[34] Hansjoachim Bluhm, "Pulsed power systems principles and applications", *Springer*, 1st edition, June 15, 2006.

[35] J. Christiansen and Ch. Schultheiss, "Production of high current particle beams by low pressure spark discharges", *Z. Phys.A 290*, pp. 35-41, 1979.

[36] B. L. Meena, M. S. Tyagi, S. S. P Rao, Alok Mishra, H. Khatun, Arvind Jakhar, Mahesh Kumar, U. N. Pal and A. K. Sharma, "Pseudospark switch development for pulse power modulators", *Journal of Physics: Conference Series 114*, 2007.

[37] P. Bickel, J. Christiansen, A. Gortler, W. Hartmann, R. Kowalewicz, A. Linsenmeyer, C. Kozlik, R. Stark and P. Wiesneth, "High-repetition rate, commercial pseudospark switches for pulsed modulators", *in the Proceedings of Power Modulator Symposium, IEEE Conference Record of the 1990*, pp 232-236, 1990.

[38] K. Bergmann, M. Muller, D. Reichartz, W. Neff and R. Lenert, "The radial multichannel pseudospark switch-a long lifetime switch for high current and high voltage applications", *in the Proceedings of 1999 Pulsed Power Conference, Digest of Technical Papers, 12th IEEE International*, vol. 1, pp. 232-235, 1999.

[39] A. Naweed, J. Kiefer, M. Rohner and W. Neff, "Lifetime and switching characteristics of a high-current multichannel pseudospark", *Journal of Applied Physics*, vol. 86, No. 12, pp. 6673-6676, December 15, 1999.

[40] Peter G. Bickel, Jens Christiansen, K. H. Frank, Andreas Goertler, Werner Hartmann, Claudius Kozlik and Peter Wiesneth, "High-repetition-rate pseudospark switches for pulsed high-power lasers", *in the Proceedings SPIE 1503, Excimer Lasers and Applications III*, vol. 167, September 1, 1991.

[41] BL Meena, SK Rai, MS Tyagi, UN Pal, M Kumar and AK Sharma, "Characterization of high power pseudospark plasma switch (PSS)", *23rd National Symposium on Plasma Science & Technology (PLASMA-2008), Journal of Physics: Conference Series*, vol. 208, No. 1, IOP Publishing 2010.

[42] Marin A. Gundersen and Gerhard Schaefer, "Physics and applications of pseudosparks", *NATO ASI Series B: Physics*, vol. 219, 1990.

[43] Winfried Benker, Jens Christiansen, Klaus Frank, Hartmut Gundel, Werner Hartmann, Thomas Redel, and Michael Stetter, "Generation of intense pulsed electron beams by the pseudospark discharge", *IEEE Transactions on Plasma Science*, vol. 17, No. 5, pp. 754-757, October 1989.

[44] Timothy J. Sommerer, Hoyoung Pak and Mark J. Kushner, "Cathode heating mechanisms in pseudospark plasma switches", *Journal of Applied Physics*, Issue 8, pp. 3374-3383, October 15, 1992.

[45] Shoji Kitamura, Yukio Hayakawa, Katsuhiro Miyazaki, Ken'ichi Kajiwara, Hideki Yoshida, Yuuko Yamamoto and Kouseki Akai, "Results of a 35-cm xenon ion thruster endurance test", *in the Proceedings of 27th International Electric Propulsion Conference*, Pasadena, CA, October 15-19, 2001.

[46] Dan M. Goebel, Ira Katz, James Polk, Ioannis G. Mikellides, Kristina K. Jameson, and Thomas Liu, "Extending hollow cathode life for electric propulsion in long-term missions", *American Institute of Aeronautics and Astronautics*, 5911, September 30, 2004.

[47] M. Laroussi and X. Lu, “Room-temperature atmospheric pressure plasma plume for biomedical applications”, *Applied Physics Letters*, vol. 87, No. 113902, 2005.

[48] W. Hartmann, G. F. Kirkman and M. A. Gundersen, "Current quenching in the pseudospark", *Applied Physics Letters,* vol. 58, No. 6, pp. 574-576, February 1991.

[49] Thomas Mehr, Hartmuth Arenz, Peter Bickel, Jens Christiansen, Klaus Frank, Andreas Gortler, Frank Heine, Detlef Hofmann, Roland Kowalewicz, Martin Schlaug, and Rupert Tkotz, "Trigger devices for pseudospark switch", *IEEE Transactions on Plasma Science*, vol. 23, No. 3, pp. 324-329, June 1995.

[50] Martin I. Hoffert, Ken Calderira, Gregory Benford, David R. Criswell, Christopher Green, Howard Herzog, Atul K. Jain, Haroon S. Kheshgi, Klaus S. Lackner, John S. Lewis, H. Douglas, Lightfoot, Wallace Manheimer, John C. Mankins, Michael E. Mauel, L. John Perkins, Michael E. Schlesinger, Tyler Volk, and Tom M. L. Wigley, "Advanced technology paths to global climate stability: energy for a greenhouse planet", *Science*, vol. 298, No. 5595, pp. 981-987, November 1, 2002.

[51] Sheikh Dastgeer, Jae Koo Lee, Hyun Chul Kim, and Young Hwan Kim, "Efficiency improvement of high-pressure microplasma by an electron beam", *IEEE Transactions on Plasma Science*, vol. 9, No. 5, pp. 837-843, October 2001.

[52] Ramesh Bokka, "Carbon nanotube cold cathodes for applications under vacuum to partial pressure in helium and dry air", *Master thesis*, Auburn University, August 2011.

[53] Jun Chen, S. Z. Deng, N. S. Xu, Suhua Wang, Xiaogang Wen, Shihe Yang, Chunlei Yang, Jiannong Wang and WeikunGe, "Field emission from crystalline copper sulphide nanowire arrays", *Applied Physics Letters*, vol. 80, No. 19, pp. 3620-3622, May 13, 2002.

[54] C. Wang, A. Garcia, D. C. Ingram, M. Lake, M. E. Kordesch, "Cold field emission from CVD diamond films observed in emission electron microscopy", *Electronics Letters*, vol. 27, No. 16, pp. 1459-1461, August 1, 1991.

[55] C. J. Lee, T. J. Lee, S. C. Lyu, Y. Zhang, H. Ruh and H. J. Lee, "Field emission from well-aligned zinc oxide nanowires grown at low temperature", *Applied Physics Letters*, vol. 81, No. 19, pp. 3648-3650, November 4, 2002.

[56] Y. M. Wong, S. Wei, W. P. Kang, J. L. Davidson, W. Hofmeister, J. H. Huang and Y. Cui, "Carbon nanotubes field emission devices grown by thermal CVD with palladium as catalysts", *Diamond and Related Materials*, vol. 13, No. 11/12, pp. 2105-2112, Nov/Dec 2004.

[57] Walt A. de Heer, A. Chaelain and D. Ugarte, "A carbon nanotubes field-emission electron source", *Science 17*, November 1995.

[58] Lingbo Zhu, Jianwen Xu, Yonghao Xiu, Yangyang Sun, Dennis W. Hess and C. P. Wong, "Growth and electrical characterization of high-aspect-ratio carbon nanotube arrays", *Carbon*, vol. 33, issue 2, pp. 254-258, February 2006.

[59] Michael F. L. De Volder, Sameh H. Tawfick, Ray H. Baughman and A. John Hart, "Carbon Nanotubes: Present and future commercial applications", *Science*, vol. 339, pp. 535-539, February 1, 2013.

[60] Max M. Shulaker, Gage Hills, NishantPatil, Hai Wei, Hong-Yu Chen, H.-S. Philip Wong and Subhasish Mitra, "Carbon nanotube computer", *Nature*, vol. 501, pp. 526-530, September 26, 2013.

[61] M.S. Dresselhaus, Y. M. Lin, O. Rabin, A. Jorio, A.G. Souza Filho, M. A. Pimenta, R. Saito, Ge. G. Samsonidze, and G. Dresselhaus, "Nanowires and nanotubes", *Materials Science and Engineering C*, vol. 23, pp. 129-140, 2003.

[62] Haitao Zhao, “Design and construction of carbon nanotubes (CNTs) triggered pseudospark switch,” *Ph. D Dissertation*, Auburn University, AL, 2012.

[63] J. L. Hutchison, N. A. Kiselev, E. P. Krinichnaya, A. V. Krestinin, R. O. Loutfy, A. P. Morawsky, V. E. Muraday, V. E. Muradyan, E. D. Obraztsova, J. Sloan, S. V. Terekhov, and D. N. Zakharov, "Double-walled carbon nanotubes fabricated by a hydrogen arc discharge methode", *Carbon*, No. 39, pp. 761-770, July 24, 2001.

[64] A Guerrero, J Puerta, F Gomez and F Blanco, "Synthesis of carbon nanotubes by laser ablation in graphite substrate of industrial arc electrodes", *Physica Scripta*, T131, December 5, 2008.

[65] Mukul Kumar and Yoshinori Ando, "Chemical vapor deposition of carbon nanotubes: A Review on growth mechanism and mass production", *Journal of Nanoscience and Nanotechnology*, vol. 10, pp. 3739-3758, 2010,

[66] Ondrej Jasek, Marek Elias, Lenka Zajickova, Vit Kudrle, Martin Bublan, Jirina Matejkova, Antonin Rek, Jiri Bursik, and Magdalena Kadlecikova, "Carbon nanotubes synthesis in microwave plasma torch at atmospheric pressure", *Materials Science & Engineering C*, No. 26, pp. 1189-1193, October 21, 2005.

[67] M. Chhowalla, K. B. K. Teo, C. Ducati, N. L. Rupesinghe, G. A. J. Amaratunga, A. C. Ferrari, D. Roy, J. Robertson, and W. I. Milne, "Growth process conditions of vertically aligned carbon nanotubes using plasma enhanced chemical vapor deposition", *Journal of Applied Physics*, vol. 90, No. 10, pp. 5308-5317, November 2001.

[68] Sung-Hoon Park, Paul Theilmann, Peter Asbeck, and Prabhakar R. Bandaru, "Enhanced electromagnetic interference shielding through the use of functionalized carbon nanotube-reactive polymer composites", *IEEE Transactions on Nanotechnology*, vol. 9, No. 4, pp.464-469, July 2010.

[69] Noriaki Hamada, Shin-ichi Sawada, and Atsushi Oshiyama, "New one-dimensional conductors: Graphitic Microtubules", *Physical Review Letters*, vol. 68, No. 10, pp. 1579-1581, March 9, 1992.

[70] A. Bachtold, M. Henny, C. Terrier, C. Strunk, and C. Schonenberger, J.-P. Salvetat, J.-M. Bonard, and L. Forro, "Contacting carbon nanotubes selectively with low-ohmic contacts for four-probe electric measurements", *Applied Physics Letters*, vol. 73, No. 2, pp. 274-276, July 1998.

[71] Paul L. McEuen, Michael S. Fuhrer, and Hongkun Park, "Single-walled carbon nanotube electronics", *IEEE Transactions on Nanotechnology*, vol. 1, No. 1, March 2002.

[72] T. W. Ebbesen, H. J. Lezec, H. Hiura, J. W. Bennett, H. F. Ghaemi, and T. Thio, "Electrical conductivity of individual carbon nanotubes", *Letters to Nature*, vol. 382, pp. 54-56, July 4, 1996.

[73] Qingwen Li, Yuan Li, Xiefei Zhang, Satishkumar B. Chikkannanavar, Yonghao Zhao, Andrea M. Dangelewicz, LianxiZheng, Stephen K. Doorn, QuanxiJia, Dean E. Peterson, Paul N. Arendt, and Yuntian Zhu, "Structure-dependent electrical properties of carbon nanotube fibers", *Advanced Materials*, No. 19, pp 3358-3363, 2007.

[74] F. Kreupl, A. P. Graham, G. S. Duesberg, W. Steinhogl, M. Liebau, E. Unger, and W. Honlein, "Carbon nanotubes in interconnect applications", *Microelectronic Engineering*, vol. 64, pp. 399-408, 2002.

[75] Chunsheng Du, and Ning Pan, "Supercapacitors using carbon nanotubes films by electrophoretic deposition", *Journal of Power Sources*, vol. 160, pp. 1487-1494, 2006.

[76] P. M. Ajayan, "Nanotubes from carbon", *Chemical Reviews*, vol. 99, No. 7, pp. 1787-1799, 1999.

[77] V. Datsyuk, M. Kalyva, K. Papagelis, J. Parthenios, D. Tasis, A. Siokou, I. Kallitsis, and C. Galiotis, "Chemical oxidation of multiwalled carbon nanotubes", *Carbon*, vol.46, pp. 833-840, February 4, 2008.

[78] Bo Pan and Baoshan Xing, "Absorption mechanisms of organic chemicals on carbon nanotubes", *Environmental Science & Technology*, vol. 42, No. 24, 2008.

[79] Chiara Fabbro, Hanene Ali-Boucetta, Tatiana Da Ros, Kostas Kostarelos, Alberto Bianco, and Maurizio Prato, "Targeting carbon nanotubes against cancer", *The Royal Society of Chemistry*, vol. 48, pp. 3911-3926, 2012.

[80] Boris I. Yakobson, and Phaedon Avouris, "Mechanical properties of carbon nanotubes", *Carbon Nanotubes, Topics Applied Physics*, No. 80, pp. 287-327, 2001.

[81] Min-Feng Yu, Oleg Lourie, Mark J. Dyer, Katerina Moloni, Thomas F. Kelly, and Rodney S. Ruoff, "Strength and breaking mechanism of multiwalled carbon nanotubes under tensile load", *Science*, vol. 287, pp. 637-640, January 28, 2000.

[82] Ali E. Aliev, Jiyoung Oh. Mikhail E. Kozlov, Alexander A. Kuznetsov, Shaoli Fang, Alexandre F. Fonseca, Raquel Ovalle, Marcio D. Lima, Mohammad H. Haque, Yuri N. Gartstein, Mei Zhang, Anvar A. Zakhidov and Ray H. Baughman, "Giant-Stroke, Superelastic carbon nanotube aerogel muscels", *Science*, vol. 323, pp. 1575-1578, March 20, 2009.

[83] Takuya Hayashi, Yoong Ahm Kim, Toshiharu Matoba, Masaya Esata, Kunio Nishimura, Takayuki Tsukada, Morinobu Endo, and Mildred S. Dresselhaus, "Smallest freestanding single-walled carbon nanotube", *Nano Letters*, vol. 3, No. 7, pp. 887-889, March 25, 2003.

[84] Chung-Nan, Tsai, "Selective and non-selective synthesis of carbon nanotubes (CNTs) by chemical vapor deposition (CVD) characterization: Catalysts and underlayers effects on field emission properties", *Master thesis*, Auburn University, December 8, 2012.

[85] Yonhua Tzeng, Chao Liu, Calvin Cutshaw and Zheng Chen, "Low-temperature CVD carbon coatings on glass plates for flat panel display applications", *Material Research Society*, vol. 621, 2000.

[86] Z. Donko, K. Rozsa and R. C. Tobin, "Monte Carlo analysis of the electrons' motion in a segmented hollow cathode discharge", *Journal of Physics D: Applied Physics*, vol. 29, pp. 105-114, 1996.

[87] A. Bogaerts and R. Gijbels, "Hybrid Monte Carlo-fluid model of a direct current glow discharge", *Journal of Applied Physics*, vol. 76, No. 4, pp. 2233-2241, August 15, 1995.

[88] D H Madison, A Dasgupta, K Bartschat and D Vaid, “Integral cross section for electron-impact excitation of the $3p^5 3d$ states of argon”, *Journal of Physics B: Atomic, Molecular and Optical Physics*, vol. 37, pp. 1073-1082, 2004.

[89] G. S. Voronov, "A practical fit formula for ionization rate coefficients of atoms and ions by electron impact: Z=1-28", *Atomic Data and Nuclear Data Tables*, vol. 65, No. 1, January 1997.

[90] Chester G. Wilson, Yogesh B. Gianchandani, Robert R. Arslanbekov, Vladimir Kolobov, and Amy E. Wendt, "Profiling and modeling of dc nitrogen microplasma", *Journal of Applied Physics*, vol. 94, No. 5, pp. 2845-2851, September 1, 2003.

[91] Akihiro Kono and Kazushige Iwamoto, "High-spatial-resolution multichannel Thomson scattering measurements for atmospheric pressure microdischarge", *Japanese Journal of Applied Physics*, vol. 43, No. 8A, pp. L 1010-L 1013, 2004.